AD A111161

LEVEL II

①

DTIC
S **ELECTE**
FEB 18 1982
E **D**

DEPARTMENT OF THE AIR FORCE
AIR UNIVERSITY (ATC)
AIR FORCE INSTITUTE OF TECHNOLOGY

Wright-Patterson Air Force Base, Ohio

82 02 18 059

AFIT/GAE/AA/81D-1

FINITE ELEMENT ANALYSIS OF THE VISCO-
ELASTIC INTERACTION OF THE ANNULUS
FIBROSIS AND NUCLEUS PULPOSIS WITHIN
THE HUMAN INTERVERTEBRAL JOINT

THESIS

AFIT/GAE/AA/81D-1   Leslie J. Allen
                     Capt   USAF

Approved for public release; distribution unlimited

AFIT/GAE/AA/81D-1

FINITE ELEMENT ANALYSIS OF THE
VISCO-ELASTIC INTERACTION OF THE ANNULUS
FIBROSIS AND NUCLEUS PULPOSIS WITHIN THE
HUMAN INTERVERTEBRAL JOINT

THESIS

Presented to the Faculty of the School of Engineering
of the Air Force Institute of Technology
Air University
in Partial Fulfillment of the
Requirements for the Degree of
Master of Science

by

Leslie J. Allen
Capt. USAF
Graduate Aeronautical Engineering
December 1981

Approved for public release; distribution unlimited

PREFACE

I would like to express my sincere gratitude to my thesis advisor, Dr. A. N. Palazotto, for his support and guidance during the course of this study. His unflagging interest in the project has been for me a source of inspiration and encouragement. I am also indebted to Capt. Ron Hinrichsen for his suggestions and the many hours he spent helping me to "debug" the program. Finally, I wish to thank Dr. Leon Kazarian and the staff of the Air Force Aerospace Medical Research Laboratory for sponsoring the study and providing the necessary computer resources.

Contents

List of Figures

List of Figures

(Continued)

List of Figures

(Concluded)

LIST OF SYMBOLS

$\Delta(\ )$	Small change in ( )
$(^{\circ})$	Time rate of change of ( )
$\{\ \}$	Vector
$[\ ]$	Matrix
$\{a\}$	Generalized displacements
A	Area of triangular element
$[A]$	Matrix of Poisson's ratio terms
$[B]$	Matrix which relates generalized displacements to nodal displacements
$[D]$	Material property matrix
E	Young's modulus
$\{F^e\}$	Nodal forces due to initial strain
G	Elastic shear modulus
$[K]$	Stiffnes matrix
Kp	Kilopond (= 2.2536 lb/ = 9.80665N)
n	Summation limit
N	Shape Function
$\{P\}$	Applied force vector
q_0, q_1	Visco-elastic parameters
r	Radial coordinate direction
sq cm	Square centimeter
t	Time
$[T]$	Transformation matrix
$\{u\}$	Nodal displacement vector
u	Nodal displacement in radial direction

v	Nodal displacement in axial direction
z	Axial coordinate direction
η	Dashpot constant
ϵ	Strain
ν	Poisson's Ratio
ϕ	Fiber angle
σ	Stress
()	Tangential coordinate direction

ABSTRACT

An understanding of the mechanical properties and behavior of the intervertebral disc is critical to several current areas of research. Among these are the study of the effects of extreme gravitational forces on the air crews of high performance aircraft, the related problem of spinal injuries due to aircraft ejection, and the study of disc degeneration. This study was undertaken in order to construct a realistic analytical model of the intervertebral joint using the finite element approach.

Experiments have shown that healthy intervertebral joints exhibit creep when subjected to axial load. A previous study of this time dependent behavior employed a simplified visco-elastic model of the disc which neglected its inhomogeneity. Though the homogeneous model successfully simulated the externally observed response of its joint, it could not adequately portray the internal response of the disc, especially the interaction of the annulus fibrosis and the nucleus pulposis.

The focus of this investigation is the behavior and interaction of the nucleus and annulus under loading, noting, in particular, the role of the annulus as a restraining mechanism on the nucleus. An axisymmetric finite element model is employed which incorporates a linear visco-elastic constitutive relation for the annulus and

nucleus. This relation is based upon a three-parameter Kelvin solid. The visco-elastic constants are found by matching one dimensional axial experimental data with this two dimensional model. The nucleus, which is composed of a series of concentric lamellae of collagen fibers, has been modelled as a 12 ply structure of orthotropic material. The cortical bone, trabecular bone, and the bony end plate are assumed to be isotropic and linearly elastic.

Results are presented which depict the displacement profiles and stress redistributions occurring as a consequence of the interaction of the annulus, nucleus, and bony end plate under axial compressive loading. Horizontal profiles of each of the stress components are presented for three regions of the joint; the trabecular bone, its bony end plate, and the intervertebral disc. The latter profiles clearly show the importance of the nucleus as a load carrying structure and the action of the annulus in restraining the outward flow of the nucleus.

Also presented are the variations in stress with time in three of the lamina of the annulus (an inner, middle, and outer ply). Results indicate that the orthotropic material properties of the annulus have a significant impact upon its time dependent behavior and should be included when modelling the joint.

A FINITE ELEMENT ANALYSIS OF THE
VISCO-ELASTIC INTERACTION OF THE NUCLEUS
PULPOSIS AND ANNULUS FIBROSIS WITHIN THE
HUMAN INTERVERTEBRAL JOINT

I. INTRODUCTION

1.1 Purpose

The purpose of this thesis is to construct a realistic analytical model of the human intervertebral joint using the finite element approach. It is an extension of an earlier work (Ref 10) which used an axisymmetric, visco-elastic model of the disc to study its time dependent behavior. This thesis further refines that model by accounting for the actual physical structure of the annulus fibrosis as well as its orthotropic properties. The focus of this investigation is the behavior and interaction of the nucleus pulposis and annulus fibrosis under axial compressive loading. The stress redistributions and displacement fields occurring as a result of the inclusion of a separate, visco-elastic annulus are investigated. Of particular interest is the role of the nucleus as a load carrying structure and the action of the annulus as as restraining mechanism on the outward flow of the nucleus under loading.

1

1.2 Background

An understanding of the mechanical properties and behavior under loading of the human intervertebral joint is pertinent to several current areas of research. Among these are the study of the effects of extreme gravitational forces on the aircrews of high performance aircraft, the related problem of spinal injuries following aircraft ejection, the treatment of congenital spinal deformities, and the development of suitable materials for disc replacement.

Although a sizeable amount of data has been gathered from experimental testing of vertebral segments, the complexity of the structure has prevented the accurate determination of material property constants for the various regions of the joint. The most complicated problems in analysis are posed by the annulus fibrosis. Composed of a series of concentric lamellae of collagen fibers, the orthotropic nature of the annulus requires that at least seven distinct material constants be determined for a linear analysis (Ref 1). Information of this type is very limited at the present time.

Experimental investigations into the load deflection behavior of the intervertebral joint were carried out by Brown (1957), Nachemson (1960), Hirsch (1965), and Rolander (1966). Galante (1967) examined the effects of inhomogeneity and anisotropy on the tensile properties of the annulus fibrosis (Ref 7). Markolf (1972) conducted

axial compression and tension tests on thoracolumbar discs
and noted significant differences in response between the
lumbar and thoracic discs (Ref 17). Kazarian, et al. (1975)
reported the creep characteristics of intervertebral joints
under constant axial load (Ref 13). More recently, Kazarian
and Kaleps (1979) presented a method for determining the
Young's Modulus and viscosity coefficient for a three-
parameter-solid model based on their earlier data (Ref 14).
Burns (1980) developed a mathematical analysis technique for
determining unique parameter values for the three-parameter-
solid model using experimental strain data.

Finite element analysis techniques have been success-
fully employed by several researchers to model the joint.
Spilker, Belytschko, and Kulak used axisymmetric finite ele-
ment models to study the time independent behavior of the
disc (Refs 21, 1, 15). Belytschko's, et al. model (1974)
assumed an incompressible nucleus in a hydrostatic state of
stress with an orthotropic, inhomogeneous, annulus fibrosis.
This study led to the conclusion that the material ani-
sotropy of the disc could not be omitted from the analysis
without causing large errors. It was also found that a
linear analysis could not account for the differences be-
tween thoracic and lumbar disc behavior or the differences
between tensile and compressive response (Ref 15). Kulak,
et al (1976) expanded on the earlier work, using a

nonlinear, elastic constitutive relation for the annulus to study the aforementioned differences.

Most recently, Hinrichsen (1980) employed an axisymmetric finite element model which included material inhomogeneity and visco-elasticity to study the creep response reported by Kazarian (Ref 10). The disc was idealized as a single, homogeneous, isotropic, linear, visco-elastic substance. This model successfully reproduced the externally observed response of the joint but due to its simplifications, could not adequately portray the internal response of the disc, in particular, the interaction of the annulus fibrosis and the nucleus pulposis.

1.3 Anatomy of the Intervertebral Joint

The human spine is a flexible column composed of a series of 24 segmented bones called the vertebrae (see Fig 1.3-A). Each vertebra consists of a ventral body and a set of posterior elements (Fig 1.3-B). One of these elements is a spinous projection, or process, which extends downward and backward. These processes may be felt as a series of bumps down the back. In addition, there are two transverse processes, one to either side, which provide attachment for muscles and ligaments. The vertebral body itself is composed of soft, trabecular bone encased in a thin shell of relatively hard cortical bone. On the upper

4

7 Cervical
Vertebrae

12 Thoracic
Vertebrae

$T_{10} - T_{11}$

5 Lumbar
Vertebrae

Sacrum

Coccyx
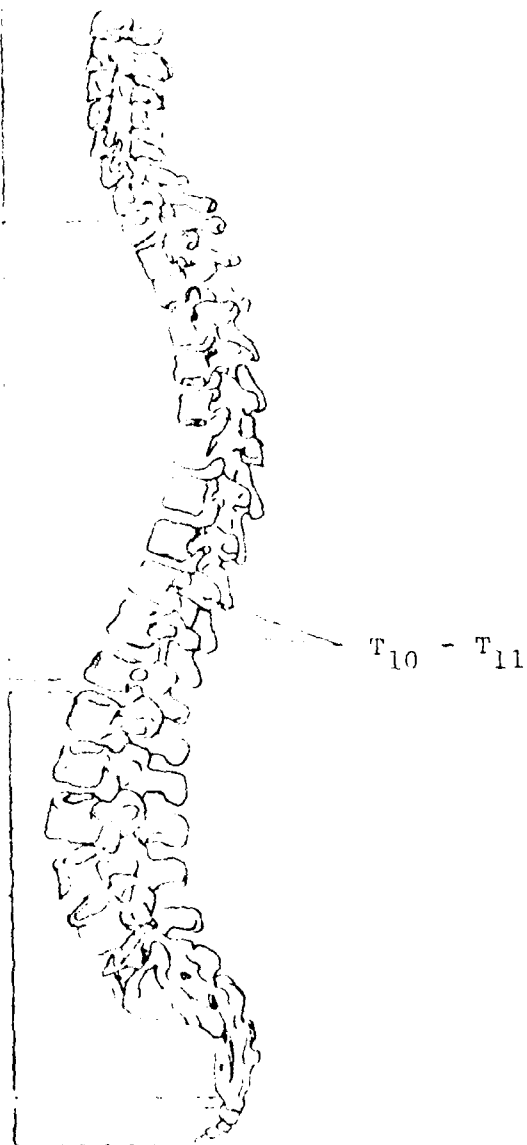
Fig 1.3-A.   Human Vertebral Column.

(from Cunningham's Textbook of Anatomy by G. J. Romanes,
University of Oxford Press)

Superior Articular Process

Inferior Articular Process

Intervertebral Disc
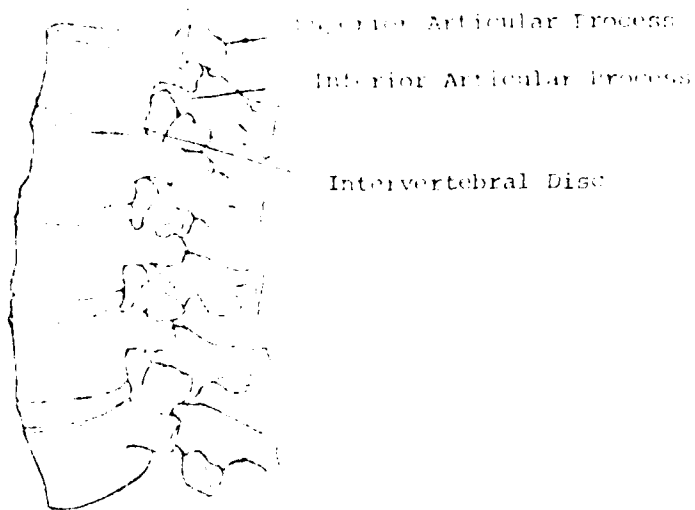
Fig 1.3-B.   Lumbar Vertebrae.

(from the CIBA Collection of Medical Illustrations
by Frank H. Netter, M.D.)

Nucleus Pulposis

Annulus Fibrosis

Top View

Lamellae

Fiber
Direction
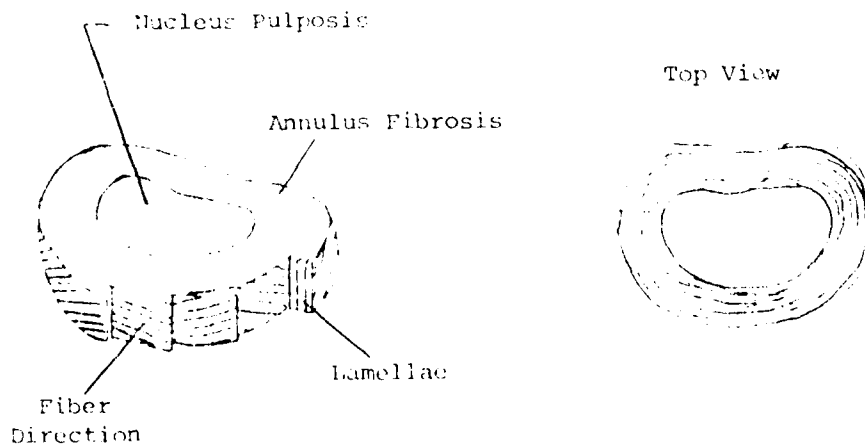
Fig 1.3-C.   Laminate Structure of Annulus.

and lower surfaces of the body are thin plates of cortical bone called bony end plates.

Between each pair of vertebrae is a cartilaginous intervertebral disc. The discs vary in size, shape, and thickness at different spinal levels. The lumbar discs are the thickest, while those in the thoracic region are relatively thin. The disc is composed of a soft center called the nucleus pulposis which is encircled by a tough, flexible, fibrocartaliginous ring called the annular fibrosis.

The nucleus pulposis is composed of a collagenous lattice enmeshed in a mucoprotein gel. Its water content ranges from 88 percent at birth to approximately 69 percent in middle age. Experiments carried out by Nachemson (Ref 18) indicate that the nucleus in normal discs behaves hydrostatically.

The annulus fibrosis is formed by a series of concentric encircling lamellae (see Fig 1.3-C). The lamellae consist of collagen fibers which have two well defined areas of orientation. The fibers run in a single direction, alternating from the previous one and aligned at approximately 30° to the horizontal (Ref 1).

Exterior to the disc proper are two ligaments; the anterior and posterior longitudinal ligaments. Although these ligaments transmit considerable force during complex loading (Ref 16), they do not appear to be significant as

load carrying structures under axial loading only.
Therefore, in order to focus on the disc interaction, the
ligaments are usually removed during axial testing of the
disc.

1.4   General Approach and Assumptions

The vertebra is modelled as an axisymmetric body which
is symmetric with respect to the centerline of the interver-
tebral disc.   Only the body itself is modelled, based upon
the assumption that little if any load is transmitted by the
anterior and posterior longitudinal ligaments during axial
loading (Ref 1).   Pictured in Fig 1.4-A are two adjacent ver-
tebrae and their intervertebral disc.   The dotted lines
indicate the truncated portion of the joint used in the
finite element model.   Fig 1.4-B is an enlarged diagram of
the model showing the various regions of the joint.   The
outer radius of the nucleus pulposis is taken to be 0.707
times the outer radius of the disc (Ref 1).

Kazarian's research (Ref 13) indicates that the ver-
tebral body alone does not exhibit creep under constant
axial load.   Therefore, it is assumed that the trabecular
bone in the vertebral core and the cortical bone in the
outer shell and end plates are linear, elastic materials.

Since the vertebral body does not appear to contribute
to the observed creep behavior of the joint, it is assumed
that the disc is the visco-elastic medium.   However, at the

8
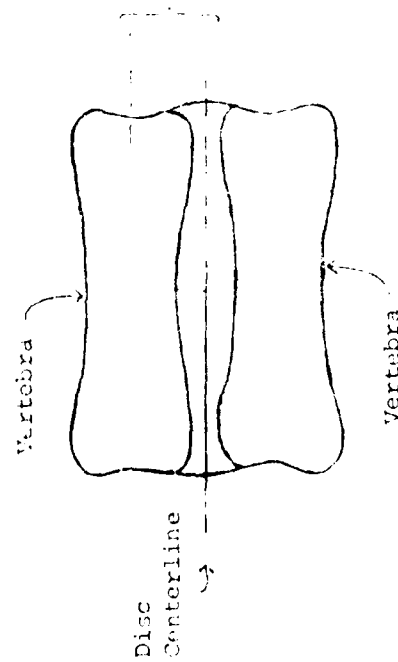
1 Vertebral Core (trabecular bone)

2 Shell (cortical bone)

3 Bony End Plate (cortical bone)

4 Nucleus Pulposis

5 Annulus Fibrosis

Fig 1.4-B. Model of Truncated Joint.
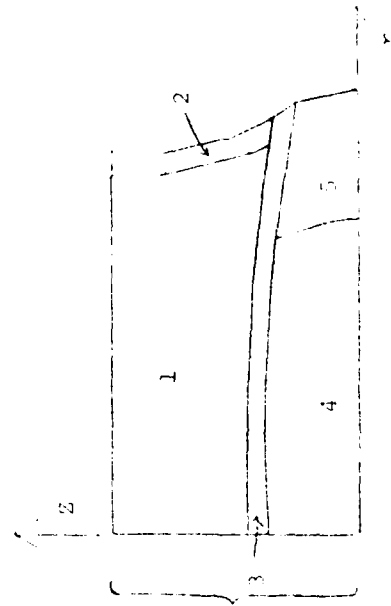
Fig 1.4-A. Side View of Two Adjacent Vertebrae and the Intervertebral Disc

9

time of this analysis, it was unknown whether the visco-elastic response should be attributed to the nucleus, the annulus, or both. As a first guess, it was assumed that the nucleus alone was the visco-elastic medium. The assumption was based upon Kazarian's (Ref 14) work with degenerated discs. The nuclei of these discs exhibited varying degrees of herniation and/or desiccation, mainly due to ageing. Kazarian reported that unlike healthy discs, the degenerated discs did not exhibit creep response. Therefore, the annulus was originally assumed to be linearly elastic. During the course of the investigation, however, it was decided to model both the nucleus and the annulus visco-elastically. The steps which led to this decision are discussed in detail in Chapter IV.

An existing finite element program was adopted for use in this investigation. The original program was written by Hinnerichs (Ref 9) to handle plane-stress, plane-strain problems in isotropic materials. Hinrichsen (Ref 10) modified the program to accommodate axisymmetric structures and to account for visco-elastic response in inhomogeneous materials. In order to account for the orthotropic proper-ties of the annulus, the program was again modified.

In the following chapter, the basic theory behind the finite element analysis method is reviewed. Included there is the derivation of the orthotropic material property matrix used to modify the existing program. The procedures

used to validate the modified program are described in Chapter III. Chapter IV describes the details of the investigation, including selection of mesh size and determination of material constants. The final results are presented in the form of displacement profiles and stress redistributions.

II. THEORY

In the following sections, the basic concepts and
equations used in finite element analysis are briefly
reviewed. The derivation of the orthotropic material prop-
erty matrix used to modify the finite element program is
discussed in Section 2.3. In the final section, an overview
of linear visco-elastic theory and the procedure by which it
is incorporated into finite element analysis is presented.

2.1 Finite Element Method

The basic concept of the finite element method when
applied to problems of structural analysis is that a complex
structure can be subdivided into a finite number of discrete
elements, in each of which the stresses or displacements can
be represented by relatively simple functions. The number
of elements in the structure must be large enough so that
the displacement function for each element closely approxi-
mates the exact displacements in that particular region.
The solution of the complete system is then represented by
an assembly of its elements. As the size of the elements
becomes small, the solution should converge to the exact
solution for the structure.

The displacement function which is chosen to represent
the behavior of the elements must meet three conditions to
assure solution convergence. First, displacements must be
continuous between adjacent elements. Second, rigid body

displacements may not cause straining of the element.
Finally, as the element size approaches zero, the strain
must reach a constant value. The simplest displacement
function which satisfies these conditions is a linear
polynomial. A polynomial of infinite order corresponds to
the exact solution. However, as the element size becomes
small, a finite polynomial provides a simple approximation
to the exact solution.

Figure 2.1-A shows a typical triangular element with
nodes 1, 2, 3 numbered in a counterclockwise direction.
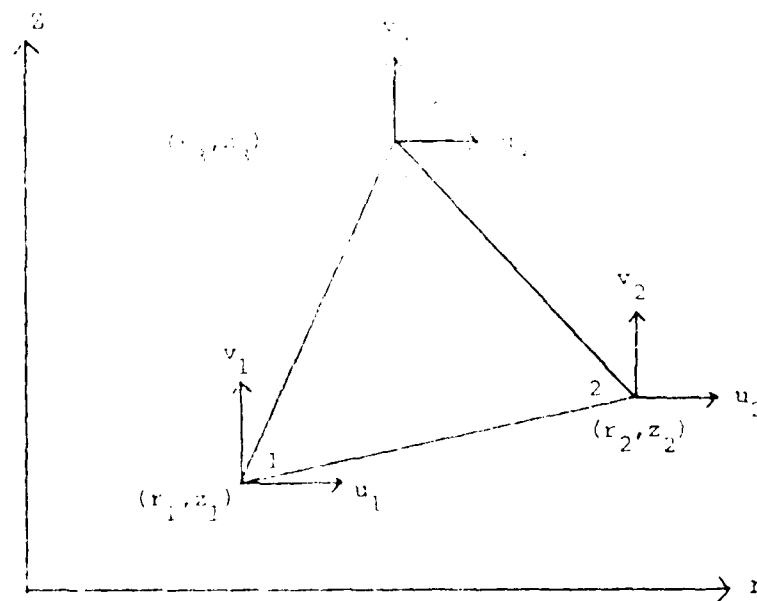
Fig. 2.1-A.

The behavior of the element is described by six degrees of
freedom which correspond to the nodal displacements:

13

$$\{u\} = \{ u_1 \quad v_1 \quad u_2 \quad v_2 \quad u_3 \quad v_3 \}^T \qquad (2-1)$$

The linear polynomial which defines the displacements within the element is

$$u = a_1 + a_2 r + a_3 z \qquad (a)$$
$$v = a_4 + a_5 r + a_6 z \qquad (b)$$
$$\qquad (2-2)$$

This may also be written in matrix form as:

$$\begin{Bmatrix} u_1 \\ u_2 \\ u_3 \end{Bmatrix} = \begin{bmatrix} 1 & r_1 & z_1 \\ 1 & r_2 & z_2 \\ 1 & r_3 & z_3 \end{bmatrix} \begin{Bmatrix} a_1 \\ a_2 \\ a_3 \end{Bmatrix} \text{ and } \begin{Bmatrix} v_1 \\ v_2 \\ v_3 \end{Bmatrix} = \begin{bmatrix} 1 & r_1 & z_1 \\ 1 & r_2 & z_2 \\ 1 & r_3 & z_3 \end{bmatrix} \begin{Bmatrix} a_4 \\ a_5 \\ a_6 \end{Bmatrix} \qquad (2-3)$$

By inversion and back-substitution into Eq 2-2 the displacement field may now be given in terms of the nodal displacements as

$$u = N_1 u_1 + N_2 u_2 + N_3 u_3 \qquad (a)$$
$$v = N_1 u_1 + N_2 u_2 + N_3 u_3 \qquad (b)$$
$$\qquad (2-4)$$

where

$$N_1 = \frac{1}{2A} \left[(r_2 z_3 - r_3 z_2) + (z_2 - z_3)r + (r_3 - r_2)z \right]$$

$$N_2 = \frac{1}{2A} \left[(r_3 z_1 - r_1 z_3) + (z_3 - z_1)r + (r_1 - r_3)z \right] \qquad (2-5)$$

$$N_3 = \frac{1}{2A} \left[(r_1 z_2 - r_2 z_1) + (z_1 - z_2)r + (r_2 - r_1)z \right]$$

and A is the area of the triangular element given by:

$$A = 1/2 \det \begin{vmatrix} 1 & r_1 & z_1 \\ 1 & r_2 & z_2 \\ 1 & r_3 & z_3 \end{vmatrix} \qquad (2-6)$$

2.2 Stress-Strain Relations for an Axisymmetric Body

The total strains at any point within an element are defined in terms of the displacement derivatives as

$$\{\epsilon\} = \begin{Bmatrix} \epsilon_\theta \\ \epsilon_z \\ \epsilon_r \\ \gamma_{rz} \end{Bmatrix} = \begin{Bmatrix} u/r \\ \partial v/\partial z \\ \partial u/\partial r \\ \partial u/\partial z + \partial v/\partial r \end{Bmatrix} \qquad (2-7)$$

By appropriately differentiating Eqs 2-4(a) and 2-4(b), the strain-displacement equation (7) may be rewritten in the following form

$$\{\epsilon\} = [B]\{u\} \qquad (2-8)$$

where

$$[B] = \begin{bmatrix} \dfrac{1}{r} N_1 & 0 & \dfrac{1}{r} N_2 & 0 & \dfrac{1}{r} N_3 & 0 \\[2mm] 0 & N_{1,z} & 0 & N_{2,z} & 0 & N_{3,z} \\[2mm] N_{1,r} & 0 & N_{2,r} & 0 & N_{3,r} & 0 \\[2mm] N_{1,z} & N_{1,r} & N_{2,z} & N_{2,r} & N_{3,z} & N_{3,r} \end{bmatrix} \qquad (2-9)$$

and $N_{1,r}$ represents the derivative of N_1 with respect to r, etc.

For a linear, elastic, axisymmetric body, the stress-strain relationship may be expressed by

$$\{\sigma\} = \begin{Bmatrix} \sigma_\theta \\ \sigma_z \\ \sigma_r \\ \sigma_{rz} \end{Bmatrix} = [D]\{\{\epsilon\} - \{\epsilon_0\}\} \qquad (2-10)$$

where $\{\epsilon_0\}$ represents any initial strains and $[D]$ is the material property matrix.

2.3 Derivation of the Orthotropic Material Property Matrix

For isotropic materials such as the cortical and trabe-cular bone, nucleus pulposis, and bony end plate, the material property matrix takes the following relatively simple form:

$$[D] = \frac{E(1-\nu)}{(1+\nu)(1-2\nu)} \begin{bmatrix} 1 & \frac{\nu}{(1-\nu)} & \frac{\nu}{(1-\nu)} & 0 \\ & 1 & \frac{\nu}{(1-\nu)} & 0 \\ \text{Symmetric} & & 1 & 0 \\ & & & \frac{(1-2\nu)}{2(1-\nu)} \end{bmatrix} \quad (2\text{-}11)$$

where ν is Poisson's ratio and E is the bulk modulus of the material.

For orthotropic materials whose principal directions coincide with the axis system the material property matrix becomes

$$[D] = C \begin{bmatrix} \frac{1-\nu_{23}\nu_{32}}{E_2 E_3} & \frac{\nu_{12}+\nu_{32}\nu_{13}}{E_1 E_3} & \frac{\nu_{13}+\nu_{12}\nu_{23}}{E_1 E_2} & 0 \\ & \frac{1-\nu_{13}\nu_{31}}{E_1 E_3} & \frac{\nu_{23}+\nu_{21}\nu_{13}}{E_1 E_2} & 0 \\ & & \frac{1-\nu_{12}\nu_{21}}{E_1 E_2} & 0 \\ \text{Symmetric} & & & \frac{G_{12}}{C} \end{bmatrix} \quad (2\text{-}12)$$

$$\text{where} \quad C = \frac{E_1 E_2 E_3}{1-\nu_{12}\nu_{21}-\nu_{13}\nu_{31}-\nu_{23}\nu_{32}-2\nu_{21}\nu_{32}\nu_{13}}$$

and where

E_1, E_2, E_3 = Young's Moduli in the 1, 2, and 3 directions

G_{12} = shear modulus in the 1-2 plane

ν_{ij} = Poisson's ratio for transverse strain in the

j-direction when stressed in the i-direction.

The annulus fibrosis, however, is an orthotropic
material whose principal directions do not coincide with the
axisymmetric body coordinate of the model. It is composed
of a series of concentric lamellae in each of which the
fibers run in a single direction, alternating from the pre-
vious one and aligned at an angle ϕ to the θ axis. Each
lamella is orthotropic in its plane with respect to coor-
dinates normal and tangent to the fiber direction.
Fig 2.3-A shows the relationship of the principal directions
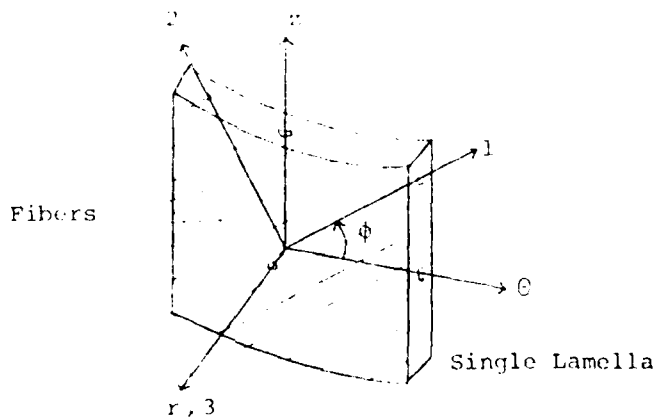to the body coordinates in a segment of a single lamella.

Fig 2.3-A. Coordinate Systems.

The stresses and strains in the principal directions
are related to those in the axisymmetric body coordinates by
the transformation matrix [T] as follows.

17

$$\begin{Bmatrix} \sigma_\theta \\ \sigma_z \\ \sigma_r \\ \sigma_{rz} \end{Bmatrix} = [T] \begin{Bmatrix} \sigma_1 \\ \sigma_2 \\ \sigma_3 \\ \sigma_{12} \end{Bmatrix} \quad \text{and} \quad \begin{Bmatrix} \varepsilon_1 \\ \varepsilon_2 \\ \varepsilon_3 \\ \gamma_{12} \end{Bmatrix} = [T]^T \begin{Bmatrix} \varepsilon_0 \\ \varepsilon_z \\ \varepsilon_r \\ \gamma_{rz} \end{Bmatrix} \quad \begin{matrix} (2\text{-}13) \\[20pt] (2\text{-}14) \end{matrix}$$

where $[T] =$
$$\begin{bmatrix} \cos^2\phi & \sin^2\phi & 0 & -2\sin\phi\,\cos\phi \\ \sin^2\phi & \cos^2\phi & 0 & 2\sin\phi\,\cos\phi \\ 0 & 0 & 1 & 0 \\ \sin\phi\,\cos\phi & -\sin\phi\,\cos\phi & 0 & \cos^2\phi-\sin^2\phi \end{bmatrix}$$
(2-15)

Therefore, combining Eqs 2-13, 2-14, and 2-15, and noting the general relationship for stresses and strains in the principal axis direction,

$$\begin{Bmatrix} \sigma_1 \\ \sigma_2 \\ \sigma_3 \\ \sigma_{13} \end{Bmatrix} = [D] \begin{Bmatrix} \varepsilon_1 \\ \varepsilon_2 \\ \varepsilon_3 \\ \gamma_{12} \end{Bmatrix} \quad (2\text{-}16)$$

we can now derive the $[D']$ matrix which relates stresses and strains in the body axes as follows:

$$\begin{Bmatrix} \sigma_\theta \\ \sigma_2 \\ \sigma_r \\ \sigma_{rz} \end{Bmatrix} = [T] \begin{Bmatrix} \sigma_1 \\ \sigma_2 \\ \sigma_3 \\ \sigma_{12} \end{Bmatrix}$$

$$= [T]\,[D] \begin{Bmatrix} \varepsilon_1 \\ \varepsilon_2 \\ \varepsilon_3 \\ \gamma_{12} \end{Bmatrix}$$

18

$$= \quad [T] \; [D] \; [T]^T \begin{Bmatrix} \varepsilon_\theta \\ \varepsilon_z \\ \varepsilon_r \\ \varepsilon_{rz} \end{Bmatrix}$$

$$\text{or,} \quad \begin{Bmatrix} \sigma_\theta \\ \sigma_z \\ \sigma_r \\ \sigma_{rz} \end{Bmatrix} = [D'] \begin{Bmatrix} \varepsilon_\theta \\ \varepsilon_z \\ \varepsilon_r \\ \varepsilon_{rz} \end{Bmatrix} \qquad (2\text{-}17)$$

$$\text{where} \quad [D'] = [T] \; [D] \; [T]^T \qquad (2\text{-}18)$$

Note that in assuming that r-axis and the 3-axis are coincident, we have neglected the physical curvature of the annulus. In reality, the 1-2 plane of the lamellae is tilted with respect to the O-z plane by a small angle which varies according to position within the annulus. Fig 2.3-B is an exaggerated diagram of the annular curvature which points out the angle in question. In order to account for this angle in the [D] matrix, a second transformation would be required. However, since the angle is small ($\doteq 12°$), the $\cos^2$ and $\sin^2$ terms approach 1 and 0 respectively. The transformation matrix (Eq 2-15) essentially becomes an identity matrix. Therefore, for the purpose of this analysis, the angle of the tilt may be safely ignored.

Based upon the foregoing theory, a computer subroutine which calculates the [D'] matrix was written and incorporated into the existing axisymmetric finite element program. The subroutine, and the methods used to validate it, are described in detail in Chapter III.
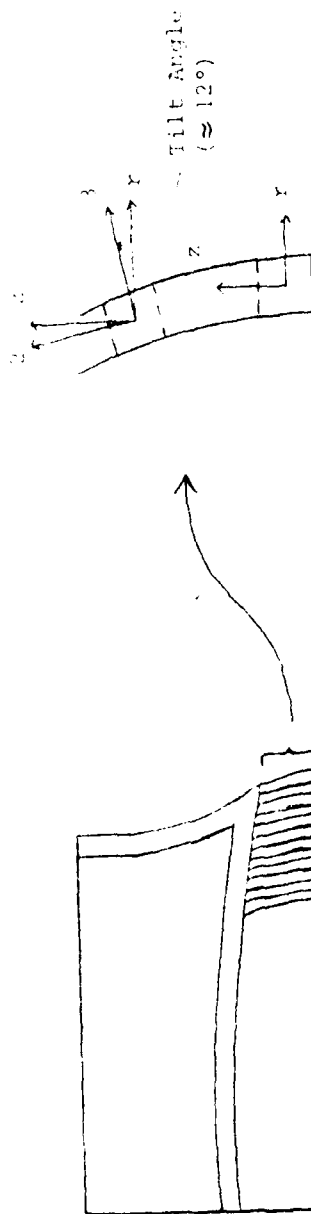
19

Tilt Angle
($\approx 12°$)

Fig 2.3-B. Annular Curvature.

2.4 Stiffness Matrix

The general equation for the elastic stiffness of an element is

$$[K] = \int_{Volume} [B]^T [D] [B] \, d \, (volume) \qquad (2-19)$$

For an axisymmetric body, the volume integral must be taken over the entire ring of material. Summing the contributions from each of the elements, the stiffness matrix for the structure is then

$$[K] = \sum_{n=1}^{N} 2\pi \int [B]^T [D] [B] \, r \, dr \, dz \qquad (2-20)$$

where N is the number of elements in the structure.

Since the [B] matrix contains terms which depend on the coordinates, straightforward integration will not suffice. However, the integration may be approximated by evaluating [B] at a centroidal point. The centroid is given by

$$\bar{r} = (r_1 + r_2 + r_3) \, / \, 3 \qquad (a)$$
$$\bar{z} = (z_1 + z_2 + z_3) \, / \, 3 \qquad (b)$$

$$(2-21)$$

and the [B] matrix evaluated at the centroid is denoted by $[\bar{B}]$. The final expression for the elastic stiffness matrix is then

$$[K] = \sum_{n=1}^{N} 2\pi \, A \, [\bar{B}]^T [D] [\bar{B}] \, \bar{r} \qquad (2-22)$$

with [D] given by Eqs 2-18, 2-12, or 2-11, depending upon the material and its orientation.

2.5 Nodal Force Vector

The external nodal forces represent a combined effect of the force acting along the whole circumference of the circle forming the element "node" (Ref 24). For the purposes of this analysis, these forces shall simply be denoted by the vector {P}.

The nodal forces due to initial strain, which are later used in the solution of the visco-elastic problem, may be expressed as

$$\{F^e\} = \sum_{n=1}^{N} \int [B]^T [D] \{\epsilon_o\} \, r \, dr \, dz \qquad (2-23)$$

The same approximation procedure which was used to integrate the stiffness equation may be employed here. The final result is

$$\{F^e\} = \sum_{n=1}^{N} 2\pi \, A \, [\bar{B}] \, [D] \, \{\epsilon_o\} \, \bar{r} \qquad (2-24)$$

2.6 Elastic Solution

Having assembled the stiffness matrix and nodal force vectors, we may solve for the displacements using the principle of virtual work. The external work done by the nodal forces is equated to the internal work done by the stresses to yield the general relation

$$[K] \{u\} = \{P\} + \{F^e\} \qquad (2-25)$$

This is the governing equation for the elastic response of a discretized structure.

2.7 Visco-Elastic Solution

Up to this point, we have dealt only with elastic materials for which, according to Hooke's Law, stress is always directly proportional to strain but independent of strain rate. Visco-elastic materials, like the nucleus pulposis, behave very differently. These materials display creep, that is, an increasing deformation under sustained load, with the rate of strain depending on the stress.

The visco-elastic behavior of materials may be modelled by various combinations of two simple elements; the spring and dashpot. The constitutive equation for a helical spring which obeys Hooke's Law is

$$\sigma = E \epsilon \qquad (2-26)$$

Similarly for the dashpot

$$\sigma = \eta \dot{\epsilon} \qquad (2-27)$$

where η is the dashpot constant and (°) denotes time differentiation.

The simplest combination of these elements is the Maxwell fluid. The elements are connected in series and the total elongation, ϵ, is a sum of the elongations in the spring and dashpot as shown in Fig 2.7-A.
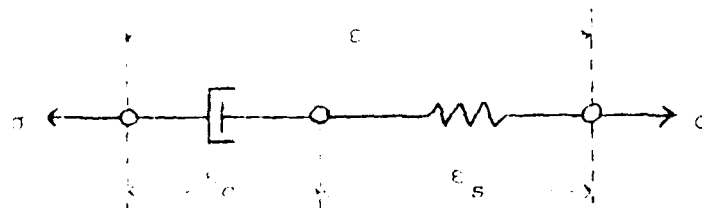

Fig 2.7-A.

23

The constitutive relation for the Maxwell fluid is

$$\dot{\varepsilon} = \frac{\dot{\sigma}}{E} + \frac{\sigma}{\eta} \qquad (2-28)$$

If the spring and dashpot are connected in parallel, the resulting model is called a Kelvin solid:
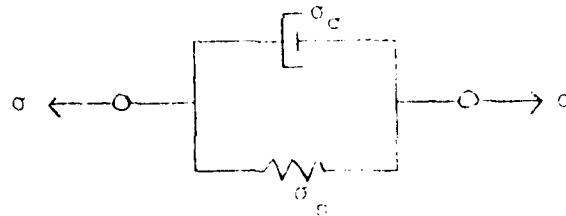
σ ←——O— —O——→ σ   Fig 2.7-B.

In this case, the total force σ is a sum of the spring and dashpot forces. The resulting constitutive relation for the Kelvin solid is

$$\sigma = E\varepsilon + \eta\dot{\varepsilon} \qquad (2-29)$$

The visco-elastic model used in this analysis is a three-parameter solid composed of an elastic spring coupled with a Kelvin solid, pictured in Fig 2.7-C.

Fig 2.7-C.

Since the instantaneous elastic deformation is dependent only on the spring, it can be separated from the creep deformation and solved by the finite element method. If the

24

constitutive relation for the three-parameter solid is
integrated over time, the resulting equation is

$$\{\Delta\epsilon_c\} = \frac{\Delta t}{q_1} \left[\frac{2}{3} \quad [A] \quad \{\sigma\} - q_0 \{\epsilon_c\} \right] \qquad (2\text{-}30)$$

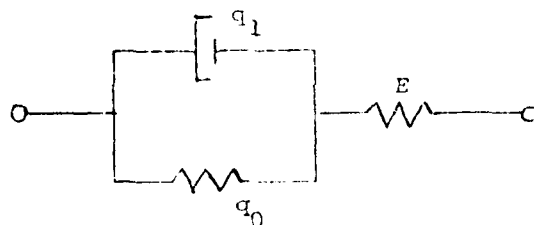where $\Delta\epsilon_c$ is the change in strain due to creep over a small
time interval and $[A]$ is given by

$$[A] = \begin{bmatrix} 1 & -1/2 & -1/2 & 0 \\ & 1 & -1/2 & 0 \\ & & 1 & 0 \\ \text{Symmetric} & & & 1/4 \end{bmatrix} \qquad (2\text{-}31)$$

The quantity $\{\Delta\epsilon_c\}$ may be considered an initial imposed
strain $\{\epsilon_0\}$. Since the initial strains enter into the
governing Eq 2-25 only in the force term $\{F^e\}$, a method of
solution to the visco-elastic problem now presents itself.
As time is increased by small increments, Δt, the governing
equation is solved at each time step for the values of $\{u\}$,
$\{\sigma\}$, and $\{\epsilon_c\}$. The values for $\{\sigma\}$ and $\{\epsilon_c\}$ are then substi-
tuted into Eq 2-30, time is incremented, and the process
continues until a maximum time is reached.

Further discussion of the application of numerical
methods to the solution of visco-elastic problems can be
found in publications by Hinrichsen (Ref 10) and Zienkiewicz
(Ref 23).

25

III. PROGRAM VALIDATION

Several checks were made to assure that the modified
[D] matrix subroutine produced the correct coefficients for
each type element. In the following section, the internal
workings of the subroutine are briefly described. The
remaining sections discuss the various methods used to vali-
date the program.

3.1 Subroutine DMATRIX

The modified subroutine works in a very simple manner.
The main program was altered so that when the data for each
element is read in, a "tag" denoting whether the element is
isotropic or orthotropic is read in as well. The tag,
called ISO in the program, is equal to zero for isotropic
elements and one for orthotropic elements. In the DMATRIX
subroutine, where the material property matrix is computed
for each element, the value of ISO determines whether an
isotropic or orthotropic [D] is computed for the element.
The procedure is diagrammed in Fig 3.1A.

```
┌─────────────────────────────┐
│  Input Element Properties   │
│                             │
│      E_i, v_ij, ISO         │
└─────────────────────────────┘
```

$ISO > 0$ Yes

No

```
┌─────────────────────┐          ┌─────────────────────┐
│  Compute ISO [D]    │          │  Compute  Ortho [D] │
│                     │          │                     │
│  From Eq 2-11       │          │  From Eq 2-18       │
└─────────────────────┘          └─────────────────────┘
```
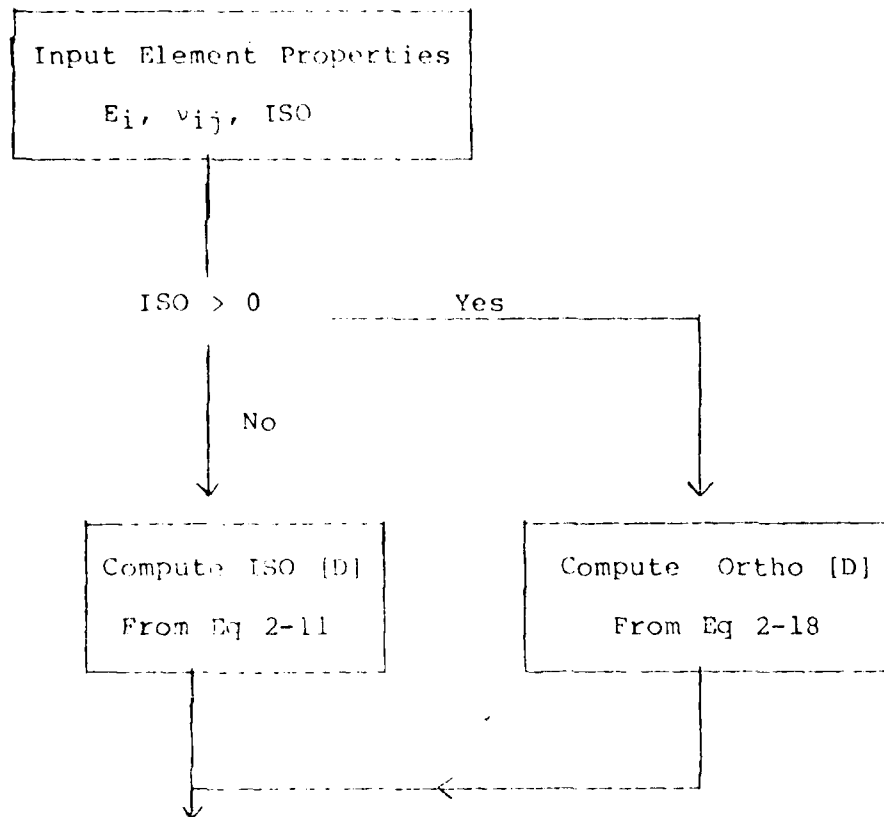
Fig 3.1-A

An initial check was made on the subroutine as a
separate entity to ascertain that data was correctly read in
and that the matrix multiplications produced the correct
results. Various values for the material constants, E_i and
v_{ij}, were input and the resulting [D] matrices compared with
hand calculations. When this check was satisfied, the
subroutine was added to the main program.

3.2 Comparison With a Known Structure

Using a mesh nearly identical to Hinrichsen's (Ref 10) final mesh, a run was made with the original program. In effect, this reproduced Hinrichsen's final results; i.e., a visco-elastic, isotropic, homogeneous disc. The same data was then run in the modified program with ISO = 0 for all elements in the disc. The results of the two runs were identical, proving that the new program had correctly computed the isotropic [D] matrix.

3.3 Internal Check

To assure that the ISO tag functions properly in the program, two more runs were made with Hinrichsen's mesh. Noting that if the angle ϕ is equal to zero and the orthotropic material constants are given by

$$E = E_1 = E_2 = E_3$$

$$\nu = \nu_{12} = \nu_{21} = \nu_{13} = \nu_{31} = \nu_{23} = \nu_{32}$$

then the [D] matrix computed from Eq 2-18 is the same as that from Eq 2-11. Therefore, if elements in a given region are tagged ISO = 1, ϕ = 0, the results should be identical to those for which the same elements are tagged ISO = 0, regardless of the value of the angle ϕ (given, of course, that the material constants are the same).

For the first run, ISO was set equal to zero in all of the elements of the disc region. For the second run, the same material constants were used, but in the annular region, ISO was set equal to one and the angle ϕ set equal

to 30°. As desired, these two runs produced identical
results.

3.4 Force Equilibrium

As a final check on the validity of the program, we
make use of the integral relation between the applied force
and the resultant stress,

$$P_z = \int_A \sigma_z \, dA \qquad (3-1)$$

This relation must hold for any horizontal cross section of
the body. Fig 3.4-A shows a side view of the joint model
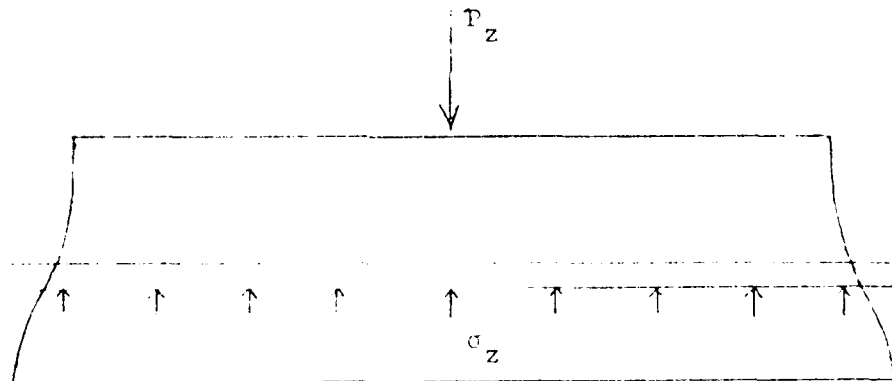through which a horizontal slice has been cut.

Fig 3.4-A. Side View of Loaded Joint.

If the σ_z stresses along the horizontal slice are
plotted versus the radius, then the area under the curve,
adjusted by a factor of $2\pi r$, must equal the applied force,
P.

Applying this test to the results of the final model of the disc, a stress profile is taken horizontally through the center of the disc at t = 0 seconds. The resulting σ_z versus r curve is shown in Fig 3.4-B. The area under the curve is calculated in three intervals; A_1, A_2, and A_3. Multiplying these areas by 2π times their respective centroidal radii, and summing, we approximate the value of the integral in Eq 3-1. These computations are shown in Fig 3.4-B.

Figure 3.4-B shows that the area approximation of the stress integral (17.7 Kiloponds) is very close to the actual applied load of 18.0 Kiloponds. Since the final model included orthotropic properties in the annulus and isotropic properties in the nucleus, we may be satisfied that the program correctly computes both types of [D] matrices.
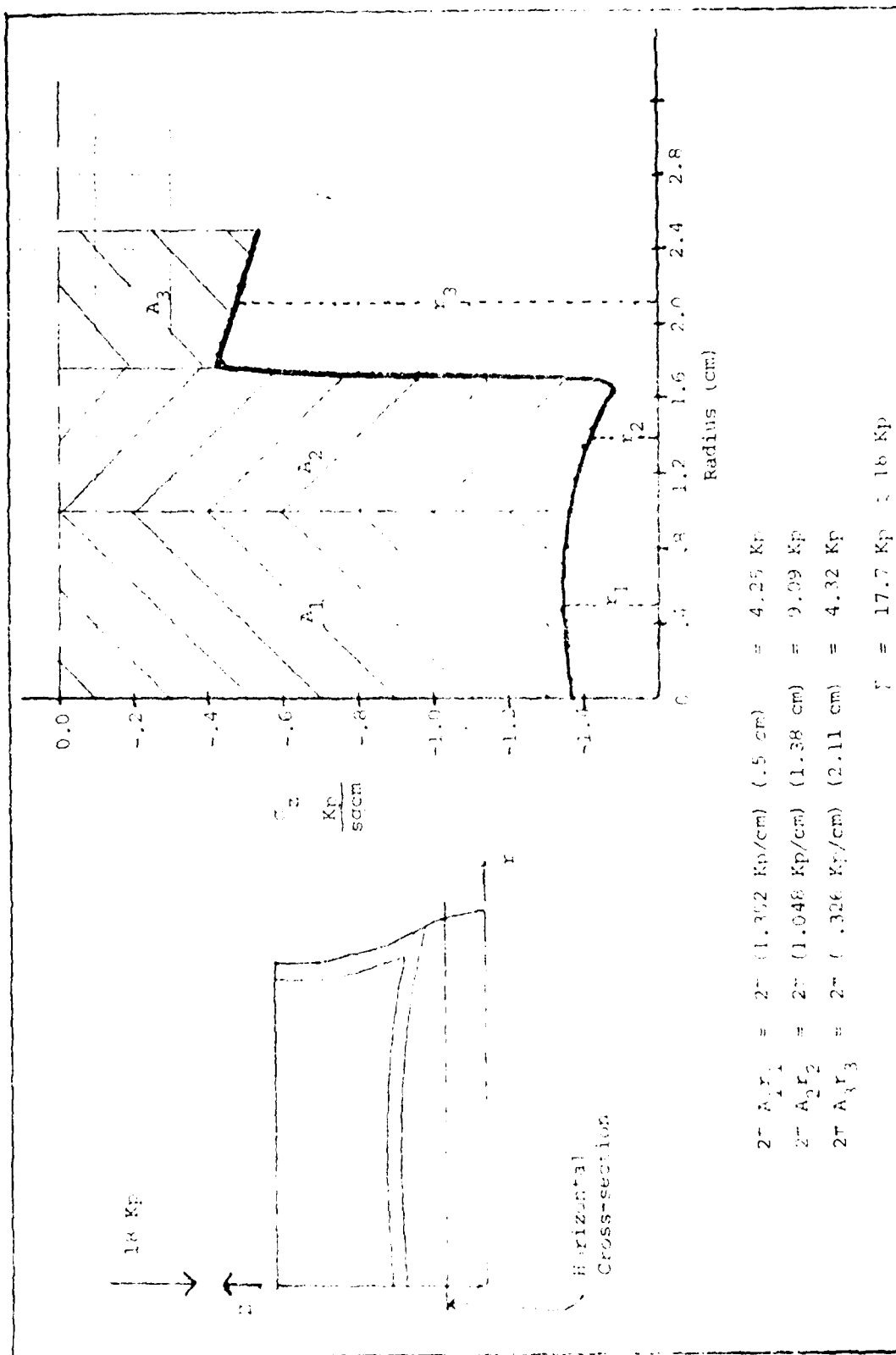
$2\pi A_1 r_1 = 2\pi (1.802 \text{ Kp/cm})(.5 \text{ cm}) = 4.25 \text{ Kp}$

$2\pi A_2 r_2 = 2\pi (1.048 \text{ Kp/cm})(1.38 \text{ cm}) = 9.09 \text{ Kp}$

$2\pi A_3 r_3 = 2\pi (.326 \text{ Kp/cm})(2.11 \text{ cm}) = 4.32 \text{ Kp}$

$F = 17.7 \text{ Kp} \approx 18 \text{ Kp}$

Fig 3.4-B. Axial Stress vs Radial and Force Computations.

IV. APPLICATION TO THE INTERVERTEBRAL JOINT

Kazarian's (Ref 14) experiments involved the testing of several types of intervertebral joint specimens. These specimens were made by cutting the vertebral bodies parallel to the lines of demarcation between the discs and the bony end plate at levels of maximum vertebral waisting. The specimens were then measured and placed in the test apparatus. Each was subjected to a dead weight load of 18.0 Kp (Kiloponds) for a period of time and the deflection of the top edge was measured (Ref 10).

Since the objective of this investigation is to determine how the inclusion of orthotropic material properties in the annulus affects the time dependent behavior of the disc, we wanted to be able to compare our results to those of Hinrichsen (Ref 10) (i.e., to an isotropic, homogeneous disc). Therefore, the same specimen used in Hinrichsen's work was used in this analysis; specimen number 65 (a T10-T11 segment). So that comparisons with Kazarian's experimental data could be made, the same 18.0 Kp load was applied to the finite element model as was applied to the test specimen.

4.1 Determination of Material Constants

The finite element model is divided into five distinct regions (refer to Fig 1.4-B). The vertebral core is assumed to be an isotropic, homogeneous material with $E = 750$ Kp/sq cm and $\nu = .25$. The material constants for

32

the cortical bone in the outer shell and bony end plate are taken to be E = 160000 Kp/sq cm and ν = .25 (Refs 1, 10).

The annulus is orthotropic, with fibers oriented at $+\phi$ and $-\phi$ to the horizontal. The angle ϕ is assumed to be 30° (Refs 11, 1). Assignment of the orthotropic material constants is based upon the values derived by Belytschko (Ref 1). He determined the values of E_1, E_2, and G_{12} that best matched Galante's (Ref 7) experimental results at various load levels. The results are plotted in Fig 4.1-A. Taking the values which correspond to an 18.0 Kp load, the material constants are as follows: E_1 = 435 Kp/sq cm, E_2 = 10.9 Kp/Sq cm, and G_{12} = 7.2 Kp/sq cm. Noting that each lamella is orthotropic in its plane with respect to coordinates normal and tangent to the fiber direction (Ref 1), we may further assume that E_3 is equal to E_2. The Poisson ratios are determined from the relation

$$\nu_{ij} E_j = \nu_{ji} E_i \qquad (4.1)$$

Assuming Belytschko's value of 0.45 for ν_{12}, we have

$$\nu_{13} = \nu_{12} = .45$$

$$\nu_{31} = \nu_{21} = .01128$$

$$\nu_{23} = \nu_{32}$$

Assuming that the material is compressible, it follows that

$$\nu_{23} \leq 1 - \nu_{13} \qquad (4.2)$$

with the equality corresponding to incompressibility. Therefore, the value of ν_{23} must be less than 0.55. For the
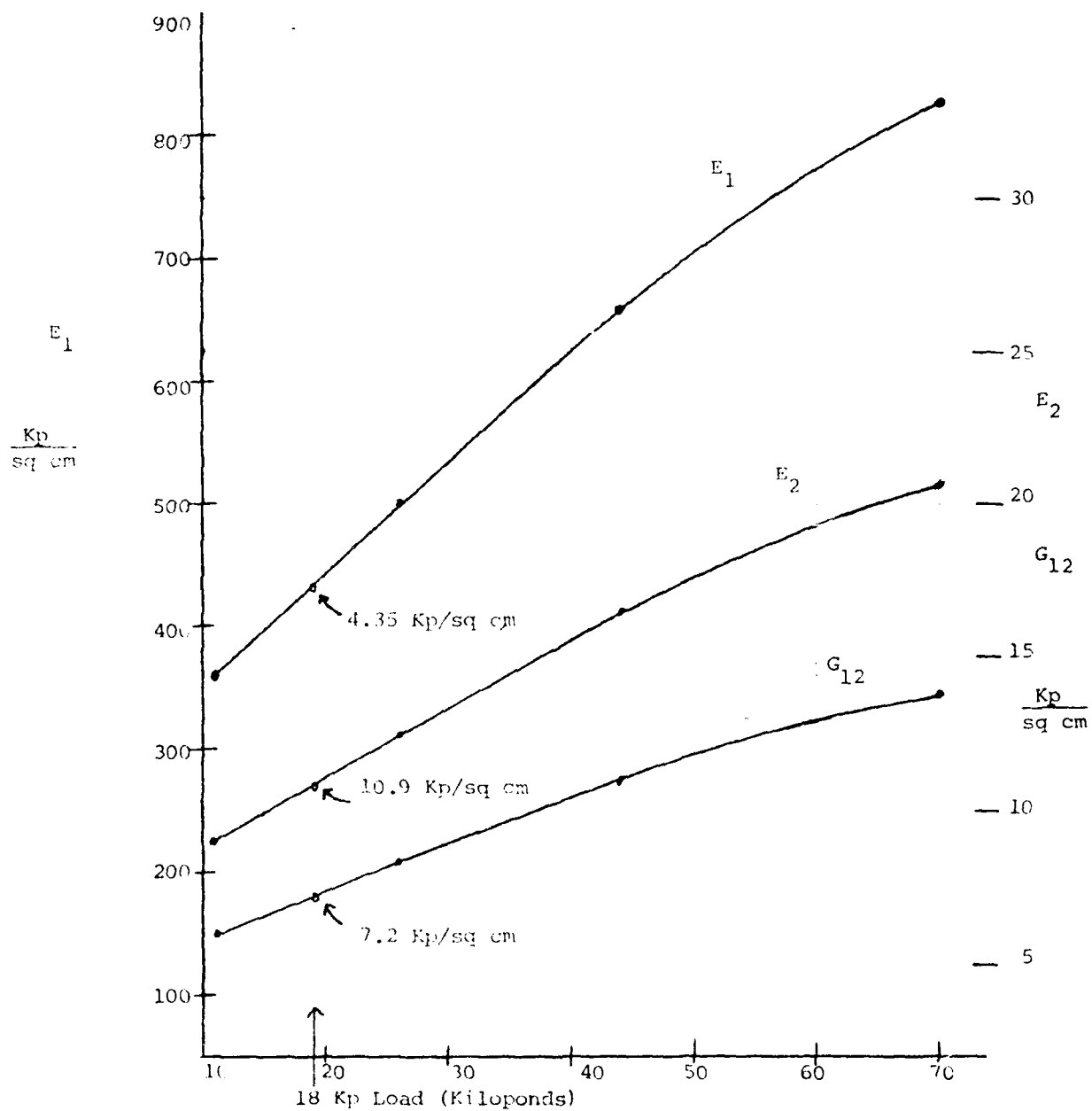
Fig 4.1-A. Material Properties of the Annulus Fibrosis.

purpose of this analysis, the value of v_{23} (= v_{32}) is assumed to be 0.45.

In the nucleus, a range of values for the Poisson's ratio were tried. To simulate a condition close to an incompressible nucleus, the value of v was set equal to 0.495. An intermediate value (the same value assumed by Hinrichsen) was set at 0.48. On the low end, v was set equal to .333 to simulate the very deformable nature of the nucleus material. Noting that the instantaneous displacement of the top edge of the model is dependent on the value of the Bulk Modulus, a trial and error method is used to find the value of E for the nucleus. The value of E is varied until the displacement of the model at $t = 0$ is equal to the experimental displacement. It was found that the experimental displacement of 0.014 cm could be matched by the model using any value of v with an appropriate value of E. These pairs of values are sho below.

$$v = .495 \qquad E = 1.58 \ kp/sq \ cm$$

$$v = .48 \qquad E = 6.2 \ kp/sq \ cm$$

$$v = .333 \qquad E = 35.0 \ kp/sq \ cm$$

At this point, only the visco-elastic constants, q_0 and q_1, remain to be determined. The procedure is similar to the method described above for finding the bulk modulus. In this case, the displacement versus time curve of the top edge of the model is compared to the experimentally determined curve. Hinrichsen found that the slope of the curve

is controlled by the value of q_1, while the q_0 value tends to influence the maximum displacement. By varying the values of q_0 and q_1 in conjunction with one another, it is possible to match the exact shape of the experimental curve with the finite element model, given that all other model assumptions are reasonably accurate. As will be seen in Section 4.4, the experimental curve cannot be matched when the annulus is assumed to be elastic.

4.2 Mesh Sizes

Four different mesh sizes were employed in this analysis. The initial mesh, pictured in Fig 4.2-A, is very similar to the mesh developed by Hinrichsen (Ref 10) and satisfies the requirement that the stresses within the joint vary smoothly from region to region. The mesh contains 224 elements and 133 node points. Note that the bottom edge of the model is constrained from axial displacement and that the node points along the axis of rotational symmetry are constrained from radial displacement. As discussed in Chapter III, this mesh was used to validate the modified program.

A coarser mesh (Fig 4.2-B), employing only 86 elements and 57 node points, was developed for interactive use on the computer. This mesh behaved roughly like the finer meshes but could be run more frequently, using less computer time.

The goal in modelling the annulus was to simulate as closely as possible the actual arrangement of the lamellae.

36
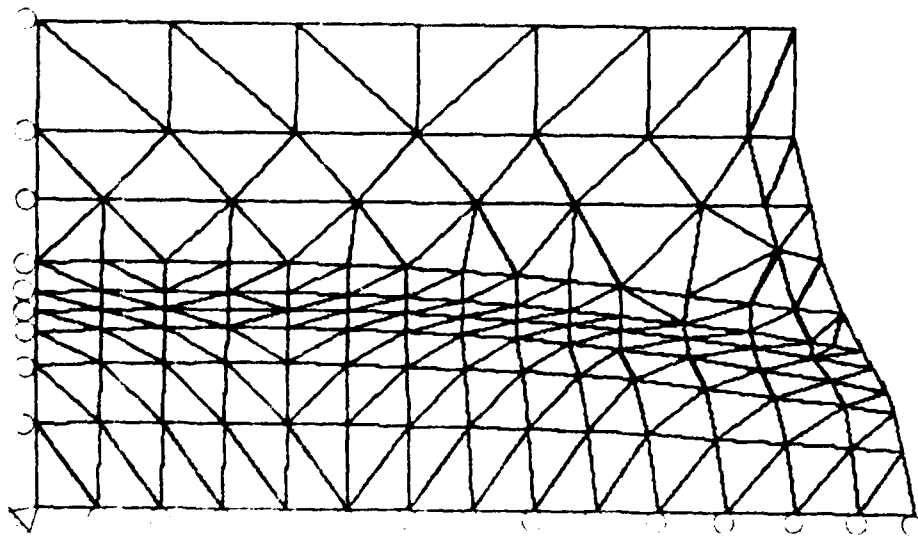
224 Elements/133 Nodes

Fig 4.2-A.   Original Mesh.
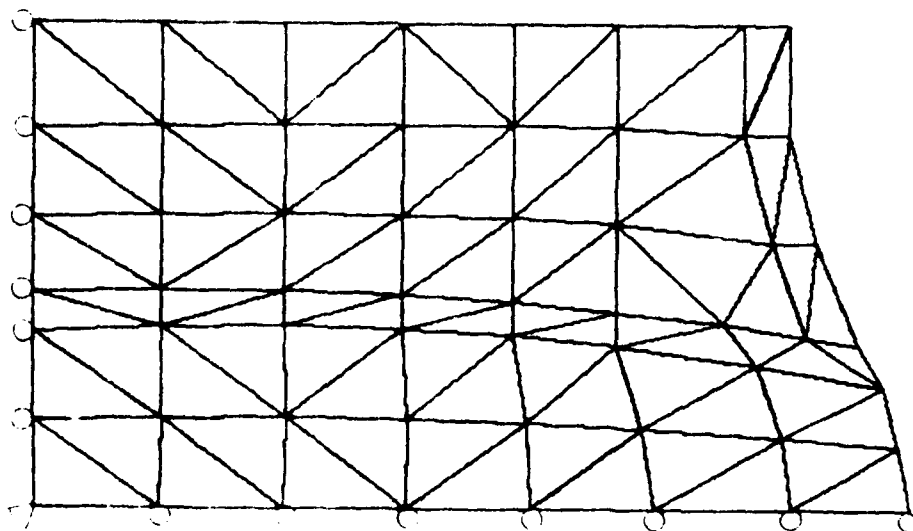


86 Elements/57 Nodes

Fig 4.2-B.   Coarse Mesh.

37

The number of fiber layers, or plies, in the annulus is esti-
mated to be 10 to 12 (Ref 2). Twelve plies were modelled in
the final mesh, bringing the total number of elements to 280
with 165 node points (Fig 4.2-D).

In order to determine whether a less refined mesh in
the annulus could be satisfactorily used to model its
behavior, an eight-ply mesh was tried with 252 elements and
149 node points (Fig 4.2-C). It was found that in order to
match the experimental initial displacement with the eight-
ply model, a slightly smaller elastic modulus in the nucleus
was required. For example, for $\nu = .495$, E was determined
to be 1.62 Kp/sq cm (compared with 1.58 Kp/sq cm for the
12-ply model). Otherwise, the two models behaved in a very
similar fashion.

In progressing from the 4-ply model to the 12-ply
model, the mesh size is systematically reduced in the annu-
lar region. Each refined mesh represents a further sub-
division within the region and therefore a more accurate
solution. The similarity in behavior of the three models
indicates that the solution is converging. Since the 8-ply
and 12-ply models use virtually the same amount of computer
time, it was decided to use the more physically accurate
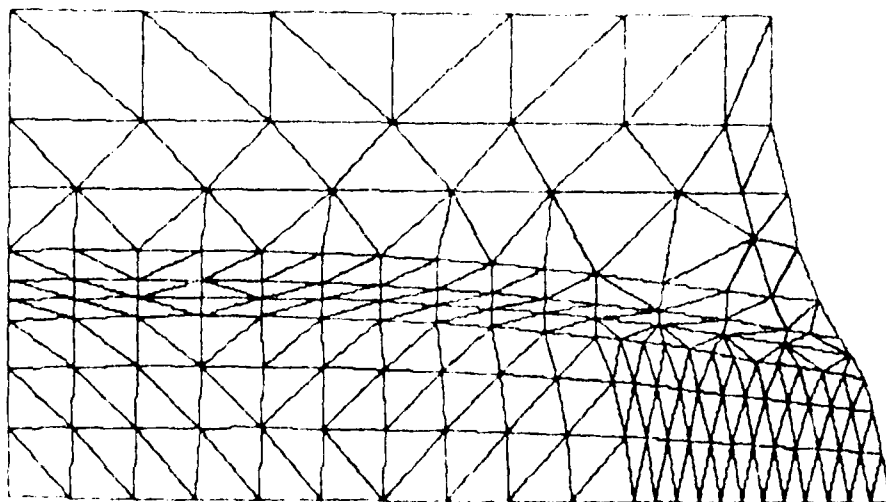12-ply model.

4.3 Initial Results: Visco-Elastic Nucleus/Elastic Annulus

As noted in Section 1.4, the disc was initially
modelled with a visco-elastic nucleus and an elastic
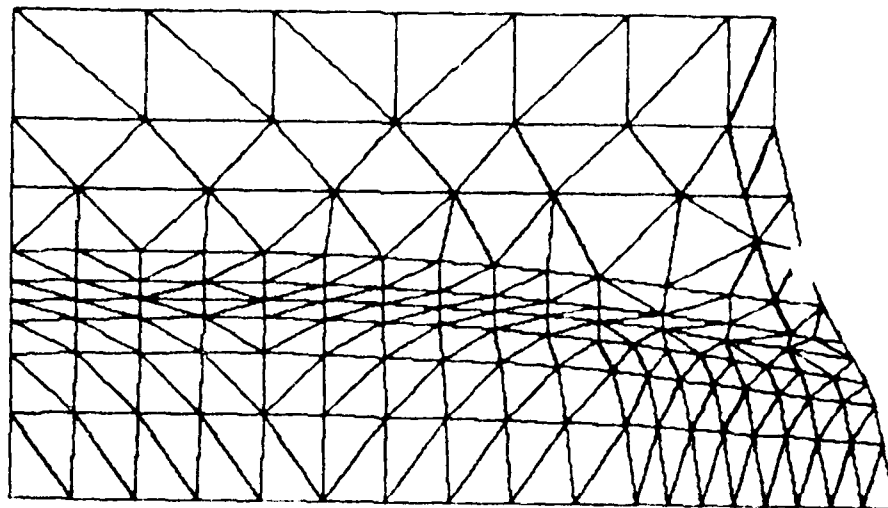
252 Elements/149 Nodes

Fig 4.2-C.   8-Ply Annulus.

280 Elements/165 Nodes

Final Mesh

Fig 4.2-D.   12-Ply Annulus.

annulus. Separate runs were made with Poisson's ratio equal to 0.495 and 0.333. Using the trial and error method previously described, appropriate values of E were found for each value of ν that allowed the initial displacement of the model to match the experimentally observed displacement.

To determine the visco-elastic parameters, Hinrichsen's final values were chosen as a starting point; $q_0 = .01$ Kp/sq cm, $q_1 = 27000$ Kp-sec/sq cm. The resulting curves, shown in Figs 4.3-A and 4.3-B, contrast sharply with the experimental curve, which rises smoothly from 0.014 cm to 0.028 cm in 20,000 seconds. For the run in which ν was set equal to 0.333, the curve levels off after 500 seconds and remains constant at approximately 0.019 cm. The curve for which ν was set equal to 0.495 appears to be even more eccentric, rising only .0001 cm in 16,000 seconds. (The roughness of this curve is not significant. It is due to the expanded interval on the Y-axis caused by computer graphics.)

In order to make these curves match the experimental curve, the method of varying q_0 and q_1 was employed. Previous analysis (Ref 10) showed that the maximum displacement increases when q_0 is decreased and that the slope increases with decreasing q_1. Therefore, the value of q_0 was progressively decreased from 0.01 to 0.0 Kp/sq cm (the zero value corresponding to a Maxwell Fluid). The value of q_1 was varied from 17000 to 47000 Kp-sec/sq cm. The results, plotted in Fig 4.3-C for $\nu = .333$, show that the
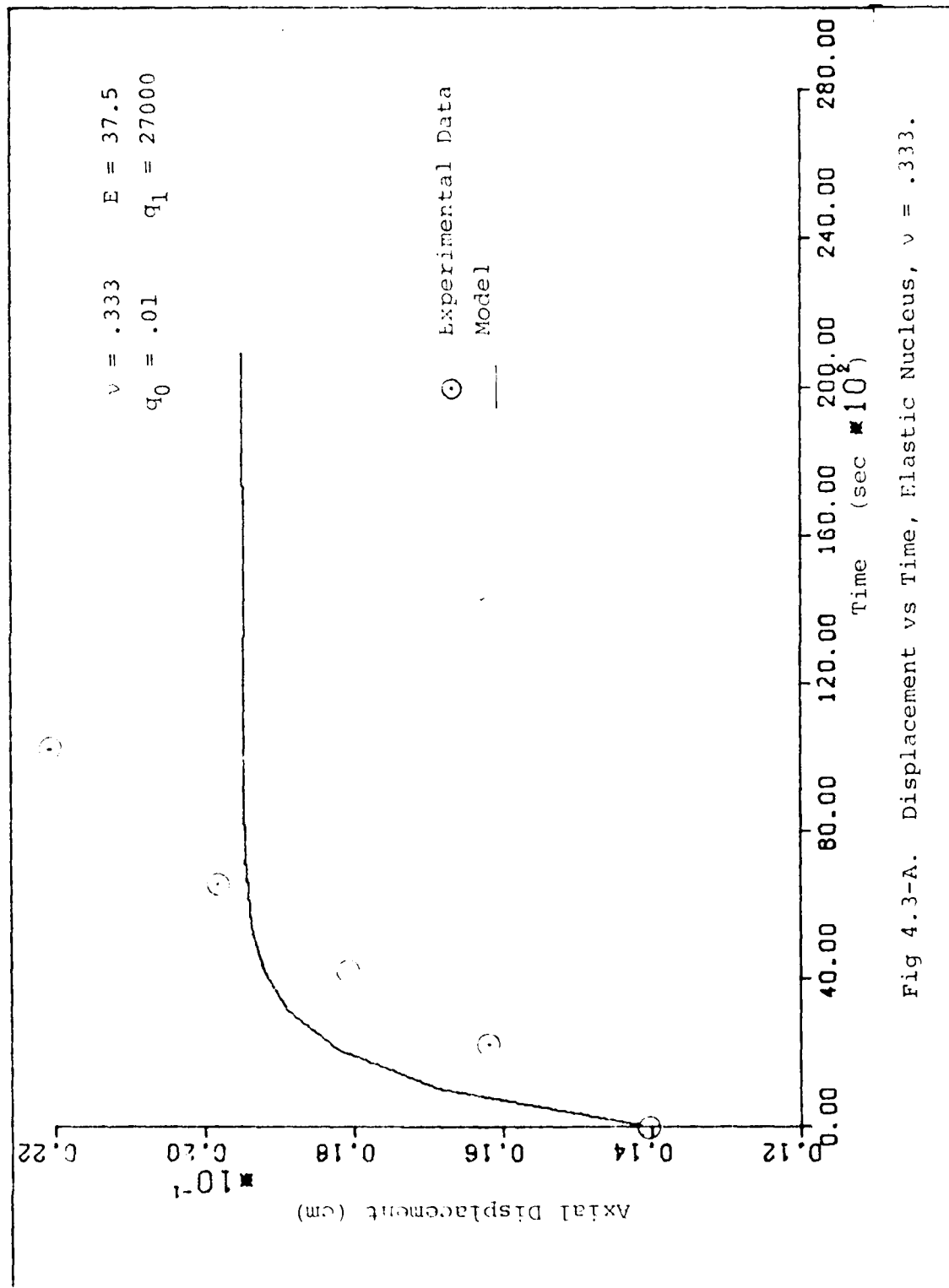
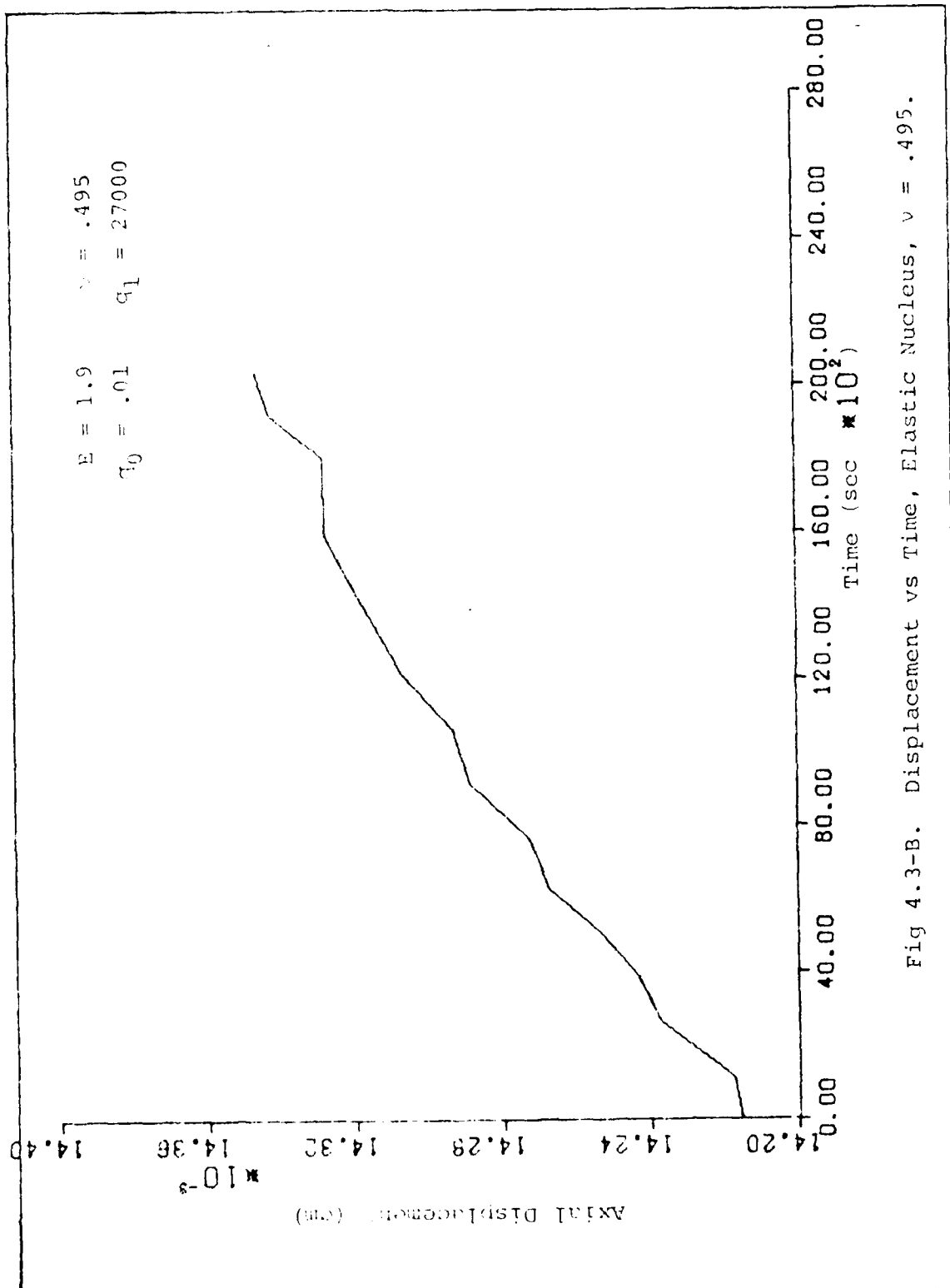Fig 4.3-A. Displacement vs Time, Elastic Nucleus, ν = .333.

ν = .333   E = 37.5
q_0 = .01 q_1 = 27000

$\odot$ Experimental Data
——— Model

Axial Displacement (cm) $\times 10^{-1}$

Time (sec $\times 10^2$)

41

Fig 4.3-B. Displacement vs Time, Elastic Nucleus, $\nu = .495$.

$E = 1.9$ $\nu = .495$

$\tau_0 = .01$ $q_1 = 27000$

Time (sec $* 10^2$)

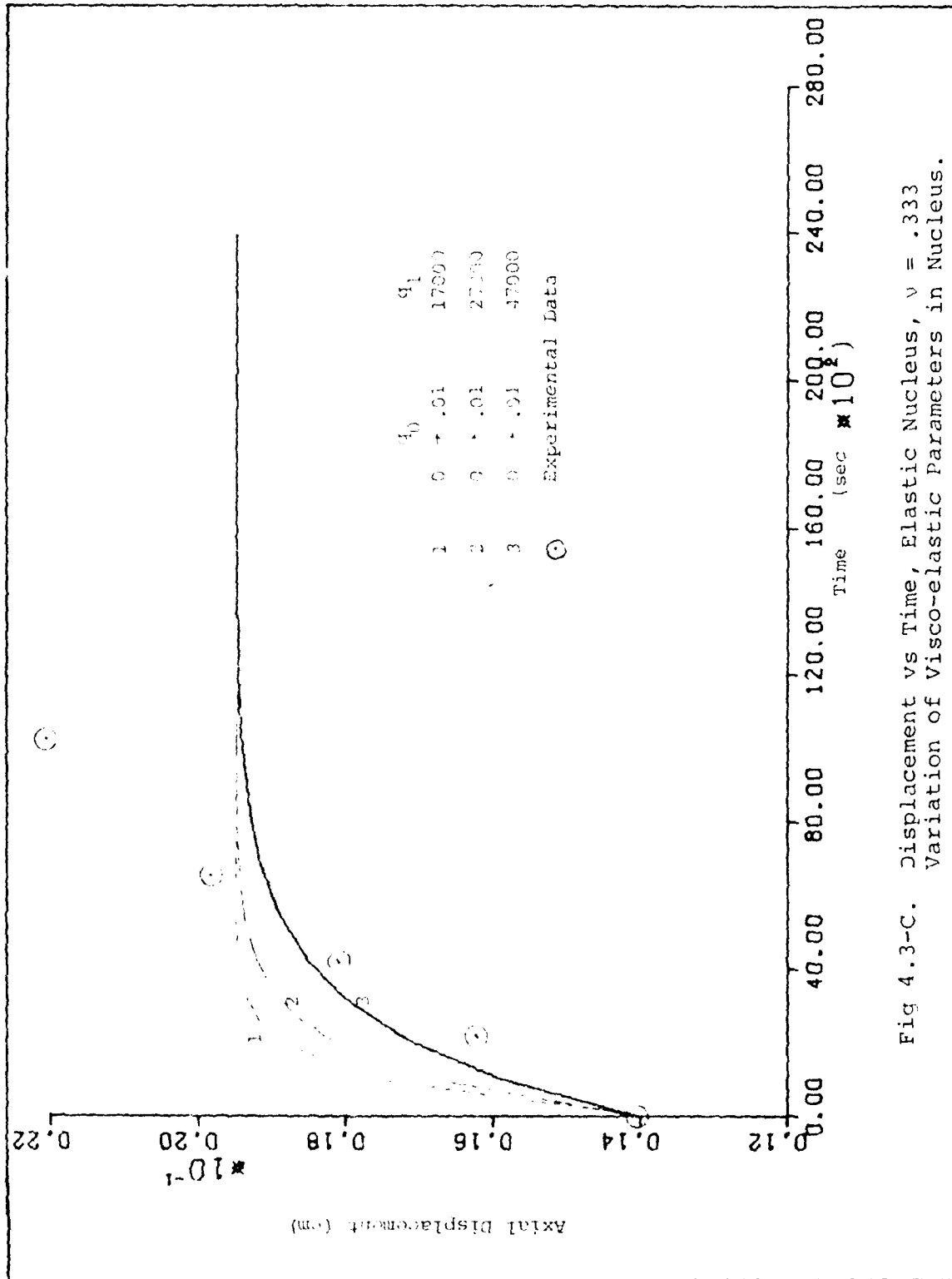Axial Displacement (cm) $* 10^{-3}$

Fig 4.3-C. Displacement vs Time, Elastic Nucleus, $\nu = .333$
Variation of Visco-elastic Parameters in Nucleus.

43

curves were unaffected by changes in q_0, regardless of the value of q_1. Similar results were obtained with $\nu = .495$. No matter how the q parameters were varied, the maximum displacement that could be achieved by the model was .0195 cm. In other words, the overall disc model appeared to be too stiff to allow further displacement.

Several approaches to the problem were considered. One option was to change the values of the orthotropic material constants in the annulus. However, these constants (with the exception of ν_{23} and ν_{32}) were based upon previous experimental work. Even if inaccurate, the means were lacking to determine seven additional constants. The value of ν_{23} ($= \nu_{32}$), on the other hand, had been chosen arbitrarily to satisfy Equation 4-3. Therefore, a range of ν_{23} values were tried, from 0.33 to 0.45. The effect on the maximum displacement was negligible.

At this point, an entirely different approach was taken. Since the stiffness of the annulus appeared to be preventing further deformation of the disc, it was decided to determine how "soft" the material constants in the annulus would have to be made to match the experimental displacements. By stipulating that the ratio of E_1 to E_2 in the annulus remain constant, the value of E_1 could be varied without affecting the values of ν_{12}, ν_{13}, etc. (reference Eq 4-1). Recalling that the nucleus had been observed to behave hydrostatically under axial load, it was assumed

to have the same bulk modulus as water. A Poisson's ratio of .333 was chosen to simulate the deformable, gel-like nucleus material. It was reasoned that if the value of E_1 required to match the experimental displacement were unreasonably small, it could be concluded that the nucleus as well as the annulus must be modelled visco-elastically to match experimental results. This did indeed prove to be the case. The value of E_1 was varied from 4350 to .435 Kp/sq cm. The resulting maximum displacements were far below the experimental value.

Based upon these findings, it was decided to model the entire intervertebral disc visco-elastically. The final results of this analysis are presented in the following chapter.

4.4 Final Model: Visco-Elastic Disc

Once the decision was made to model both the nucleus and the annulus visco-elasticaslly, the remainder of the investigation proceeded smoothly. Values of E in the nucleus had already been determined for both ν = .333 and ν = .495. It remained to find the values of q_0 and q_1 in the nucleus and annulus. It should be pointed out at this point that visco-elastic constitutive equations have yet to be derived for orthotropic materials. The annulus is effectively being modelled here as orthotropically elastic but isotropically visco-elastic.

45

Following the procedure previously outlined, the visco-
elastic parameters were varied until the model matched the
experimental displacement versus time curve. Fig 4.4-A shows
some intermediate results obtained by varying q_0 and q_1 as
well as the final match. The values of q_0 and q_1 which best
represent the data are shown below.

ν (nucleus)	q_0 (nucleus, annulus)	q_1 (nucleus, annulus)
0.333	1.2	85000
0.495	1.5	85000

Fig 4.4-B

Note that the same visco-elastic constants were used in
both the nucleus and annulus. This is most likely untrue,
since the materials in each region are different
visco-elastically. However, it is not possible to improve
upon these values with the method at hand. The problem is
that we have four unknowns (the q values in the annulus and
nucleus) and only one equation; the experimentally observed,
one-dimensional displacement of the disc. Therefore,
although we might find other sets of q values by trial and
error which produce a curve match, there would be no way to
determine which set is the more accurate. As a matter of
curiosity, other sets were tried. Not surprisingly, it was
found that the experimental curve could be matched by a
variety of q values. For example, using the coarse mesh and
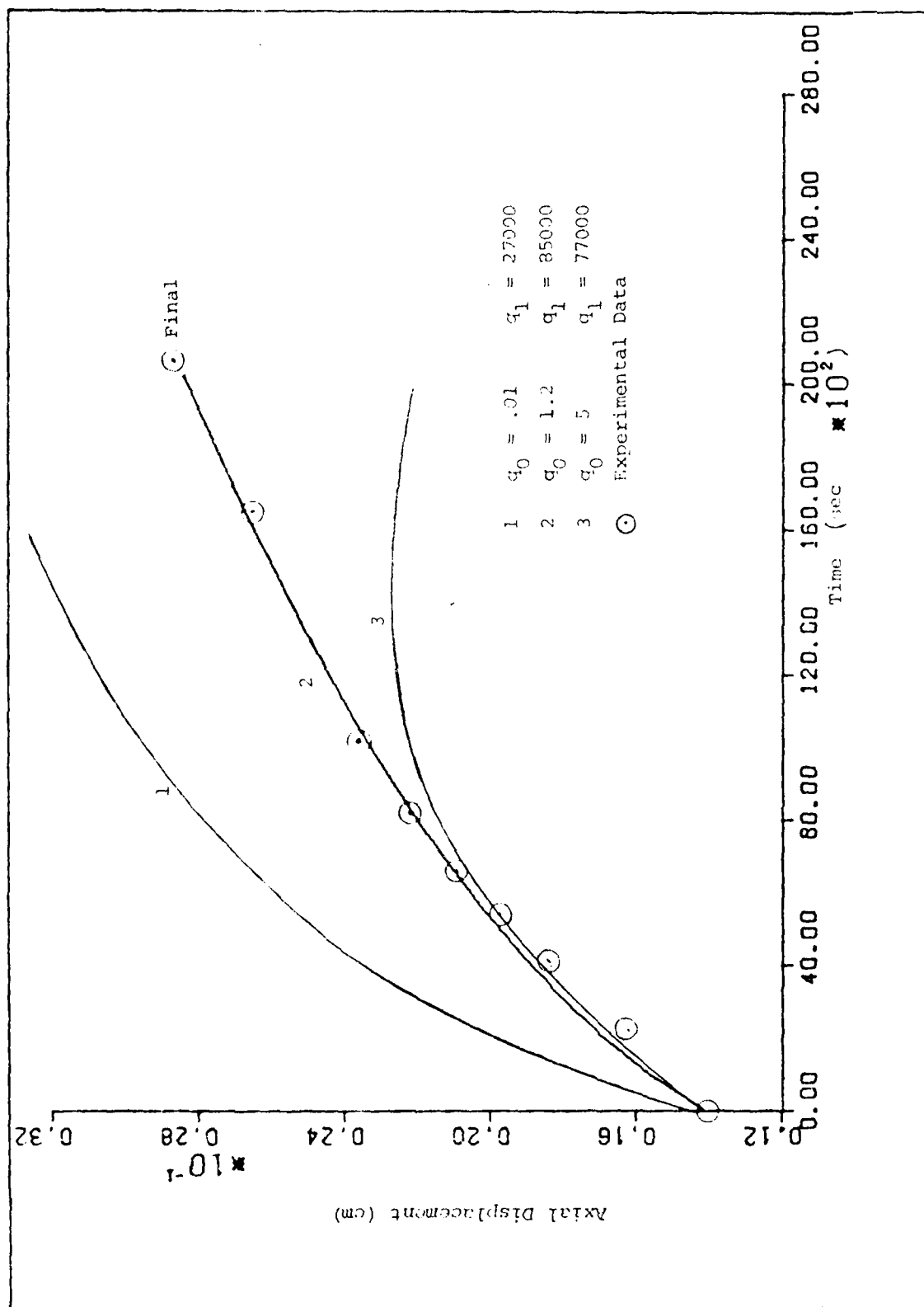a ν value of .333, the curve was matched by the following

46

Fig 4.4-A. Visco-Elastic Nucleus and Annulus.

Final

1	$q_0 = .01$	$q_1 = 27000$
2	$q_0 = 1.2$	$q_1 = 85000$
3	$q_0 = 5$	$q_1 = 77000$
⊙	Experimental Data	

Time (sec $*10^2$)

Axial Displacement (cm)

$*10^{-1}$

0.32   0.28   0.24   0.20   0.16   0.12

0.00   40.00   80.00   120.00   160.00   200.00   240.00   280.00

parameters:

	Nucleus		Annulus	
	q_0	q_1	q_0	q_1
Set #1	0.8	81000	0.8	81000
Set #2	1.0	70000	0.6	90000

In other words, the experimentally observed, one-dimensional behavior of the vertebra could be accurately simulated by the model using widely varying values for q_0, q_1, and ν. The q values which were chosen to represent the final model are those given in Fig 4.4-B.

4.5 Displacement Profiles

In order to visualize the deformations taking place throughout the joint as time increases, plots of the deformed model were made at t = 0, t = 70, and t = 170 minutes. Separate plots were generated using Poisson's ratios in the nucleus of ν = .333 and ν = .495. Since the resulting plots were virtually identical, we conclude that the displacements do not depend on the value of ν in the nucleus as long as it is paired with an appropriate E value. For this reason, only the ν = .333 plots are presented here.

Figure 4.5-A presents the undeformed shape of the model. Figures 4.5-B, C, and D are the deformed shapes at t = 0, t = 70, and t = 170 minutes, respectively. To more clearly depict the overall changes taking place, Fig 4.5-E shows the t = 170 plot overlaid on the undeformed (t = 0-) plot, with
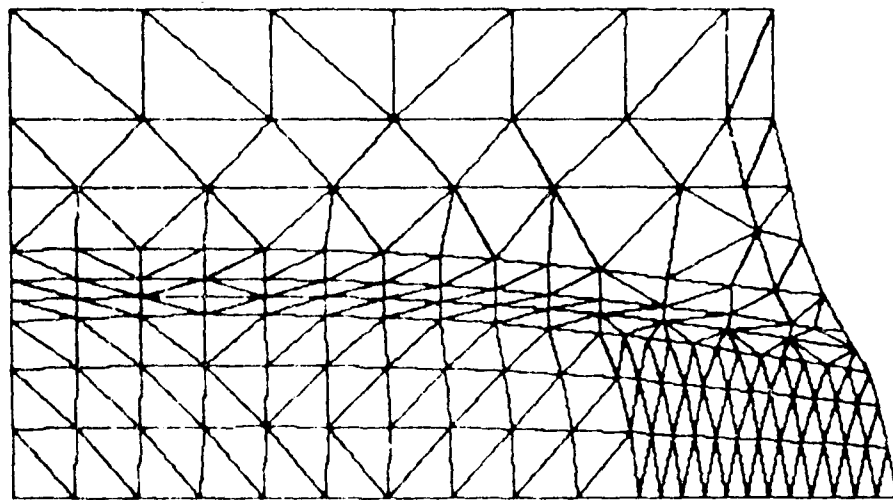
48

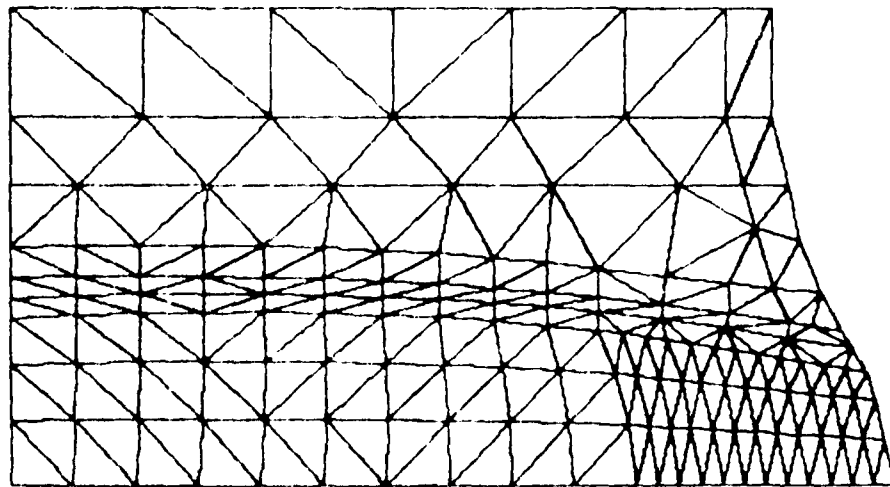Deformations Magnified x 2

Fig 4.5-A.   Undeformed Plot.

Fig 4.5-B.   Deformed Plot $t = 0^+$ Minutes.

49
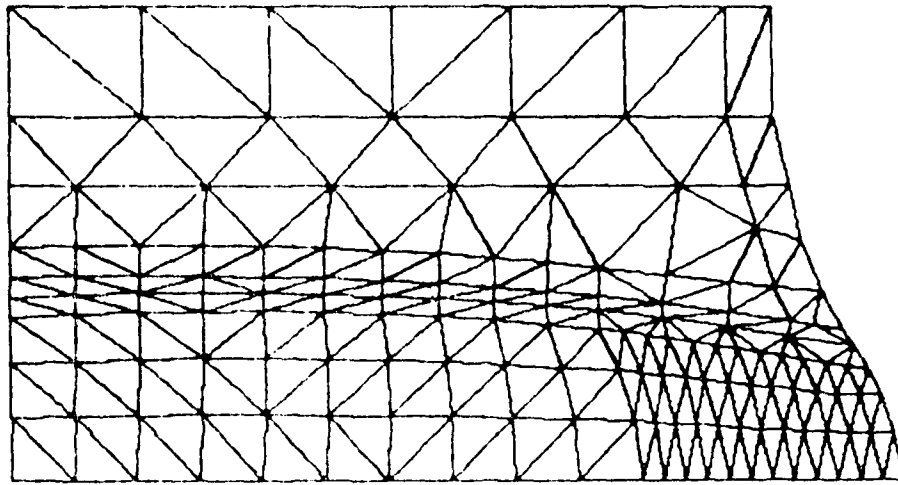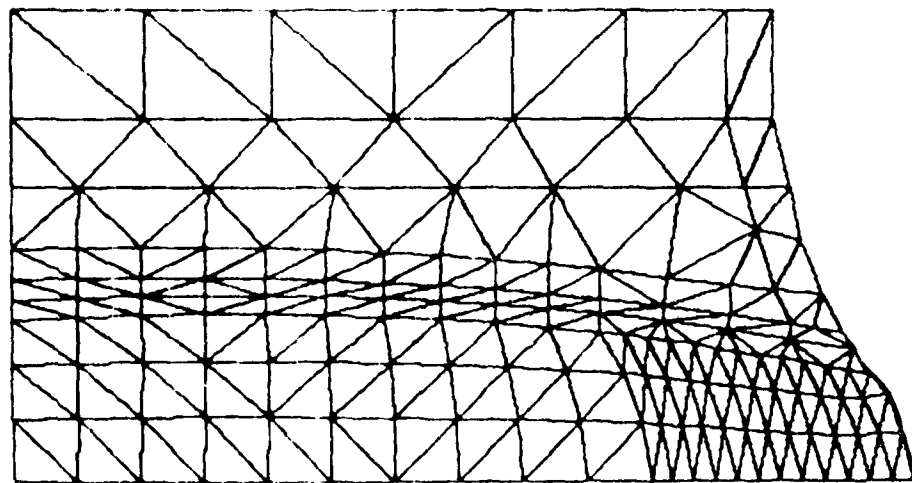
Fig 4.5-C.   Deformed Plot, t = 70 Minutes.

Fig 4.5-D.   Deformed Plot, t = 170 Minutes.
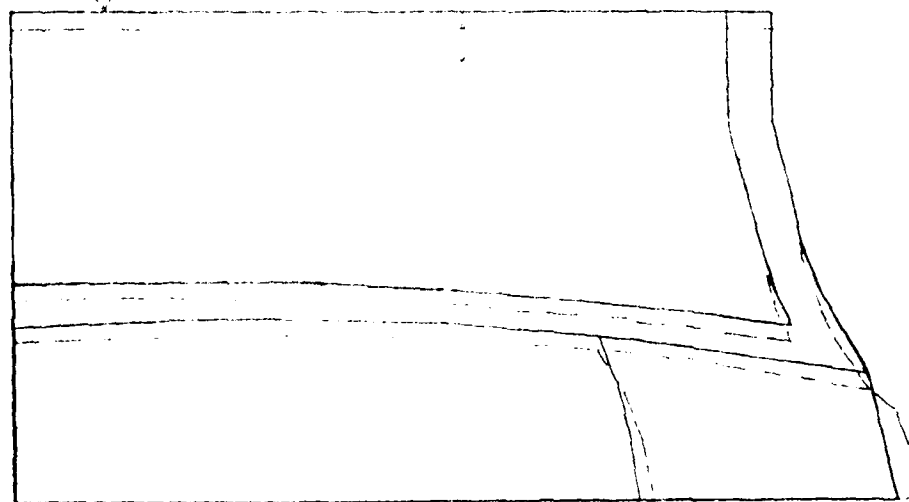
Deformations Magnified x 2

T = 0 min.

T = 170

Fig 4.5-E. Comparison of Undeformed Shape to
Deformed Shape at T = 170 Minutes.

the mesh lines deleted. Finally, for the purpose of comparison, a deformed plot of Hinrichsen's homogeneous model (Ref 10) at t = 180 minutes is reproduced in Fig 4.5-F. In each of these figures, the deformations have been magnified so that they may be more readily observed. The magnification factors are noted in the figures.

Note that there are striking differences between the behavior of Hinrichsen's homogeneous, isotropic disc and that of the present model. The homogeneous disc spreads outwardly in the radial direction with time. Its radius at the centerline increases by approximately 4% over 180 minutes of loading. On the other hand, the orthotropically modelled annulus exerts a considerable restraining force on the outward flow of the nucleus. After a similar period of time, the radius of the disc at the centerline increased only 1%.

Within the non-homogeneous disc, the annulus can be seen to be adjusting to the outward pressure of the nucleus. Since the annular fibers are firmly attached to the end plates, they are constrained from radial movement at the attach points. Therefore, the radial deformation of the annulus is greatest at the centerline of the disc. Note that the fiber layers nearest to the annulus are more directly affected by its outward flow. The inner ply consequently displace farther radially than do the outer ply. Hence, one would expect to see higher compressive stresses in the inner ply than in the outer ply. The attachment of

Deformations Magnified x 2

Orthotropic
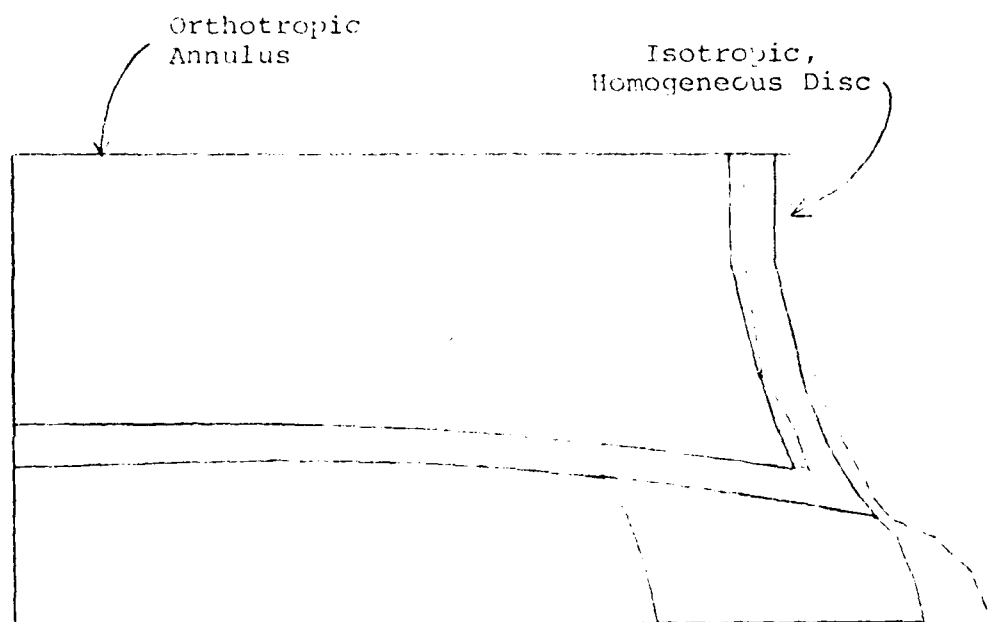Annulus

Isotropic,
Homogeneous Disc

Fig 4.5-F.   Comparison of Present Model to
            Hinrichsen's Model at t = 170 Minutes.

53

the annular fibers to the end plate should have an effect on the stresses within the endplate as well, particularly on the shear stress.

The vertebral body and the bony end plate appear to undergo virtually no deformation with time. The entire axial displacement takes place within the intervertebral disc. This is not surprising because of the large difference between the elastic modulus of bone versus that of fibrocartilage.

In the following section, the actual stress redistributions are presented and compared to those produced in the homogeneous disc model.

4.6 Stress Redistributions

Horizontal profiles of the radical, axial, hoop, and shear stress components were taken at three different joint levels; through the disc, the bony end plate, and the vertebral body. Fig 4.6-A indicates the position of these horizontal slices. To determine the effect of the Poisson's ratio in the nucleus, separate profiles were generated for $\nu = .333$ and $\nu = .495$. It was found that for the most part, the ν value had little effect upon the behavior of the model. A few differences were noted in the way that certain stress components varied with time in the disc and end plate. For example, with $\nu = .333$, the hoop and radial stresses in the nucleus increase approximately 70% over a 170 minute interval. The same stresses decrease 10% during
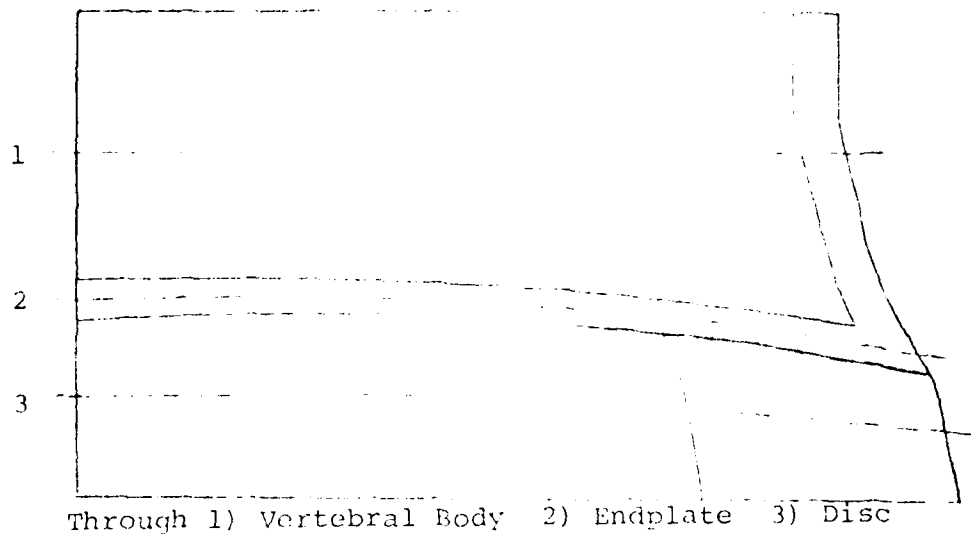
54

Through 1) Vertebral Body 2) Endplate 3) Disc

Fig 4.6-A. Horizontal Profiles.

Fig 4.6-B. Ply Profiles.

Inner

Mid   Outer
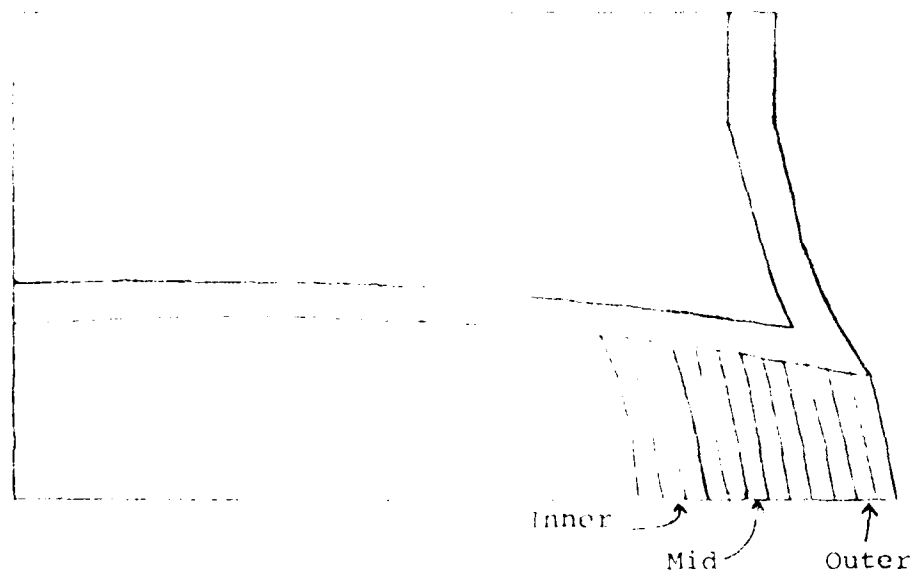
that interval when $v = .495$. These differences may be attributed to the fact that the higher value of v decreases the rate of displacement in the nucleus by limiting the direct strain. At this point a choice had to be made as to which value of v would be used in the final model. Either value could be used to match the experimental displacements and both produced similar stress profiles. It was decided that the lower value, corresponding to a deformable, gel-like solid, would provide the best model of the behavior of the nucleus. The resulting horizontal stress profiles are presented in Figs 4.6-C through 4.6-N for times varying from 0 to 170 minutes.

A second set of profiles was taken to show the stress redistributions in the individual lamella. Three separate plies are profiled; an inner ply, an outer ply, and one mid-way between (see Fig 4.6-B). The stresses are averaged over the length of the ply and plotted against time. To compensate for the effect of the alternating fiber angle, the stresses in two adjacent lamella were initially averaged together to represent the stress in a single ply. As it turned out, the stresses vary so smoothly from ply to ply that this averaging technique proved unnecessary. Therefore, the stress profiles presented in Figs 4.6-O through 4.6-R represent stresses averaged within single plies.

We first examine the stress redistributions in the disc, where the effect of the annulus-nucleus interface is immediately evident. At t=0 minutes, both the hoop and axial stresses decrease 71% across the interface (Figs 4.6-D, E). The shear stress, which is virtually zero in the nucleus, goes to .2 Kp/sq cm in the annulus (Fig 4.6-F). As time progresses, and the disc adjusts to the load, these changes become less abrupt. Comparing these profiles to similar ones made by Hinrichsen (Ref 10) of a homogeneous disc, we see that the stress magnitude and the manner in which they vary in time are very similar. The general shapes of the profiles are also the same, although the effect of the annulus is necessarily absent in the homogeneous model.

Looking at the physical structure of the annulus, one would expect its behavior to be that of a thick-walled cylindrical shell subjected to internal pressure. That is, one expects to see dominant tensile hoop stresses in the annulus as a result of axial loading and outward pressure of the nucleus. Kulak (Ref 15) demonstrated that this is, in fact, the case in lumbar discs. On the other hand, thoracic discs, such as the specimen modelled in this analysis, are relatively thinner and therefore more constrained by their end plates. Figs 4.6-E and 4.6-Q show that the annulus is in a state of hoop compression. It is acting in effect, not

like a shell, but like a ring under axial load. The magnitude of this compression is small; approaching zero at the outer edge of the annulus. This agrees with Kulak's analysis of thoracic discs. He, too, observed small hoop stresses in the annulus and compression in many of the annulus fibers.

Fig 4.6-C shows that the radial stress tends to vary smoothly across the interface at all times, though it decreases rapidly in the outer ply of the annulus. This indicates that the outer plies are under considerably less radial compression than the inner plies. The same conclusion may be drawn from Fig 4.6-O which shows 36% more radial compression in the inner ply than in the outer. Note that in the outer ply, all four stress components are fairly constant over time (Figs 4.6-O,P,Q,R). In contrast, the stresses in the inner ply (with the exception of shear) tend to increase with time. This implies that the inner lamellae do most of the work in restraining the nucleus under small loads.

In the bony end plate, the magnitude of the shear, hoop, and radial stress components is much greater than in any other region of the joint. This signifies the importance of the end plate as a structural member of the joint. Although the displacement profiles indicate that little actual deformation takes place in the end plate under axial load, it does undergo significant redistributions of stress

over time. For example, Fig 4.6-I shows that the hoop stress in the end plate increases 36% in a 170 minute interval. In contrast, the radial stress increases with time only in the region directly above the nucleus (Fig 4.6-G). The axial and shear stresses in the end plate also appear to be affected by their proximity to the annulus-nucleus interface (Figs 4.6-H, 4.6-J). It is unlikely that the abrupt peak in the axial stress curve at r = 1.9 cm is a completely accurate representation of the stress in that area. The peak may be partially due to insufficient refinement of the mesh size in that region. However, further refinement of the mesh would be very expensive in terms of computer resources. Also, it is questionable whether any degree of refinement would produce a smooth stress transition in a region where three different types of materials are joined.

In the vertebral body, the hoop and shear stresses (Figs 4.6-M and 4.6-N) are virtually constant across the radius and do not vary with time. Note that the last data point on these plots represents the stress in the thin shell of cortical bone which encases the vertebral core. The stresses in the shell, like those in the bony end plate, did vary with time. It is significant to note that the cortical shell is in a state of hoop tension. That is, its behavior is that of a classical shell. In both the vertebral body and the end plate, the axial stress tends to decrease with radius, but dramatically increases at the outer edge of the

joint. This supports the idea that the load is transmitted mainly through the cortical shell and end plate to the nucleus, which then acts as the primary load carrying structure of the joint.
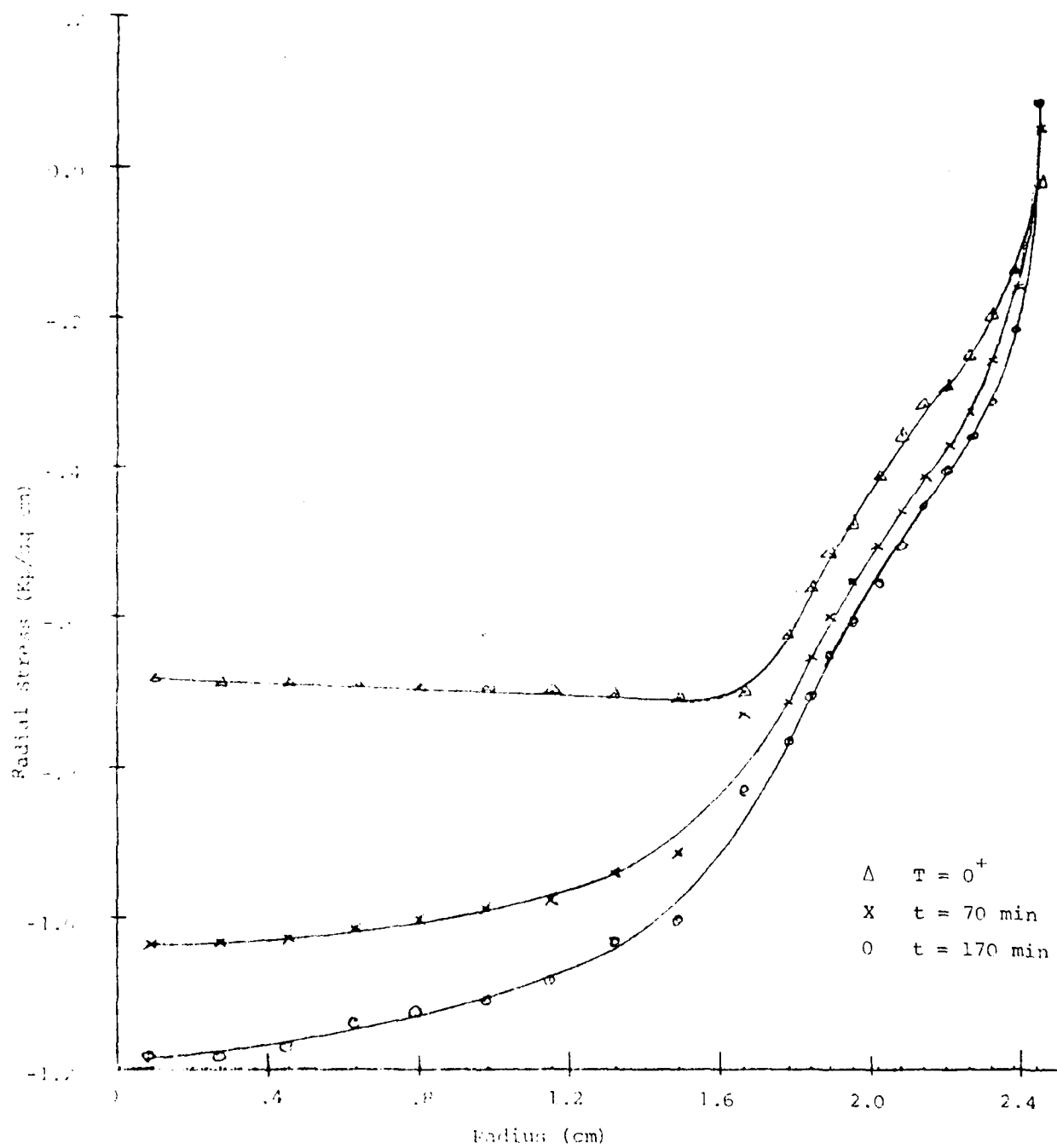
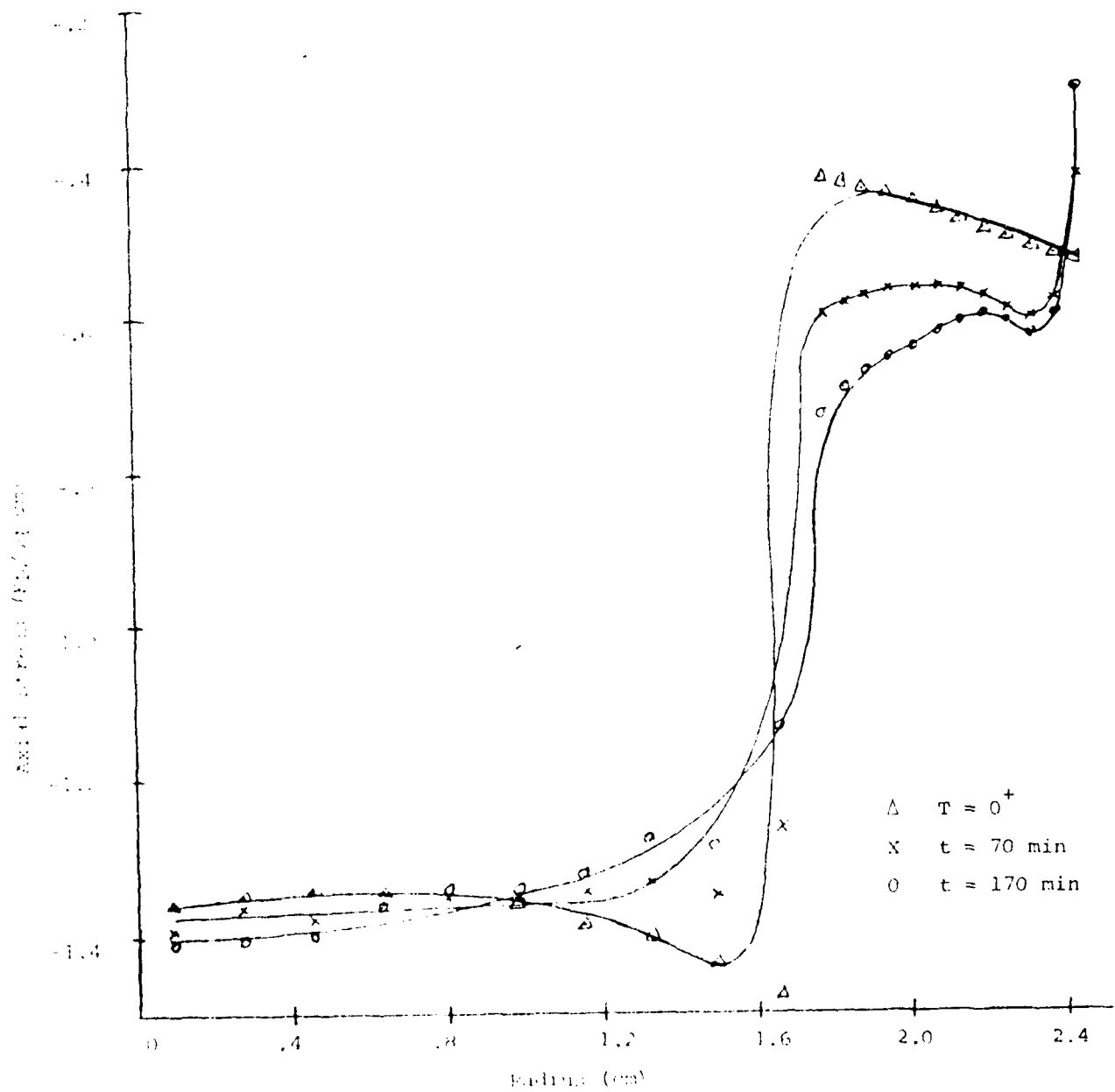Fig 4.6-C.   Radial Stress, Disc.
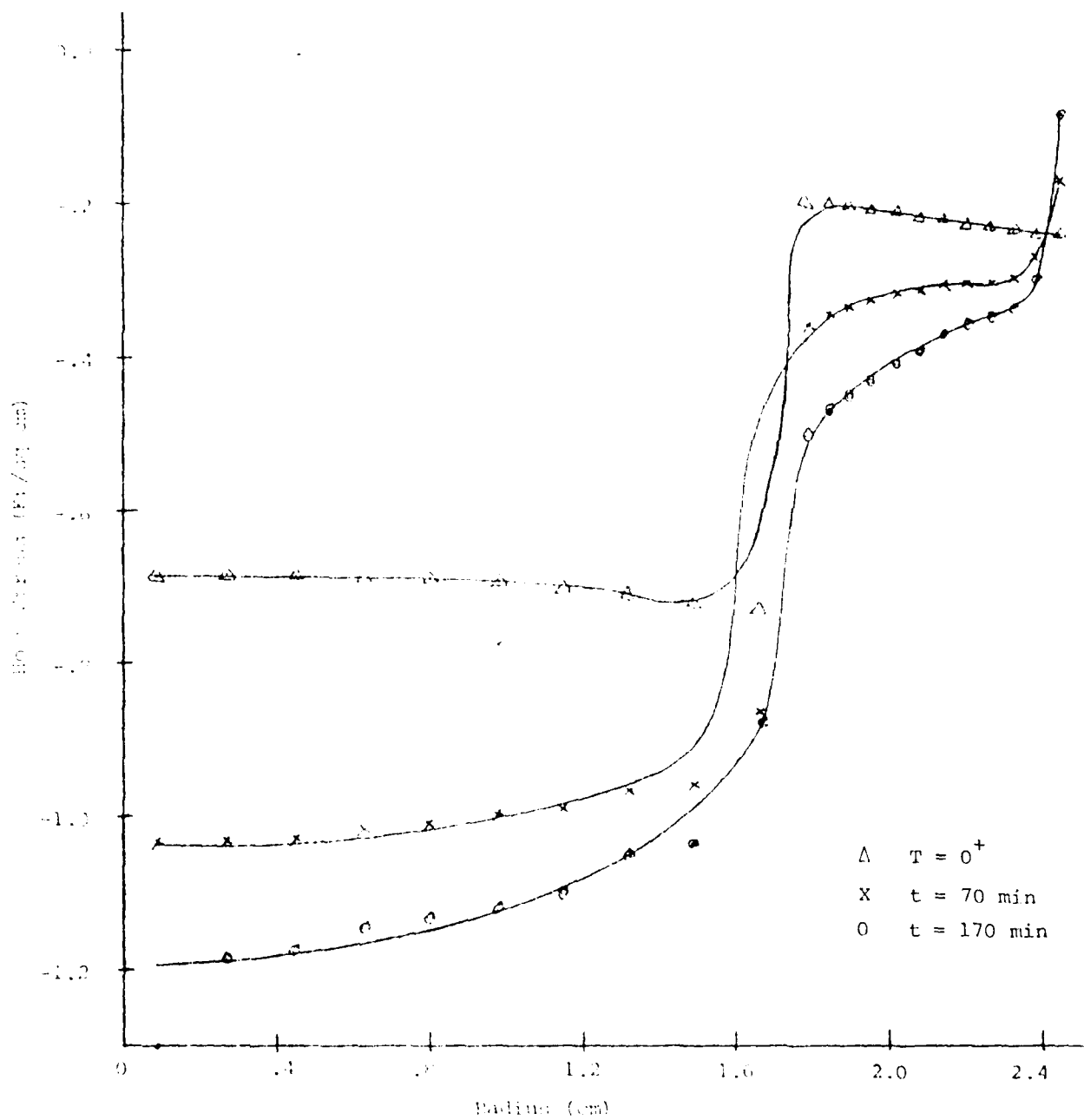
61

Fig 4.6-D.   Axial Stress, Disc.
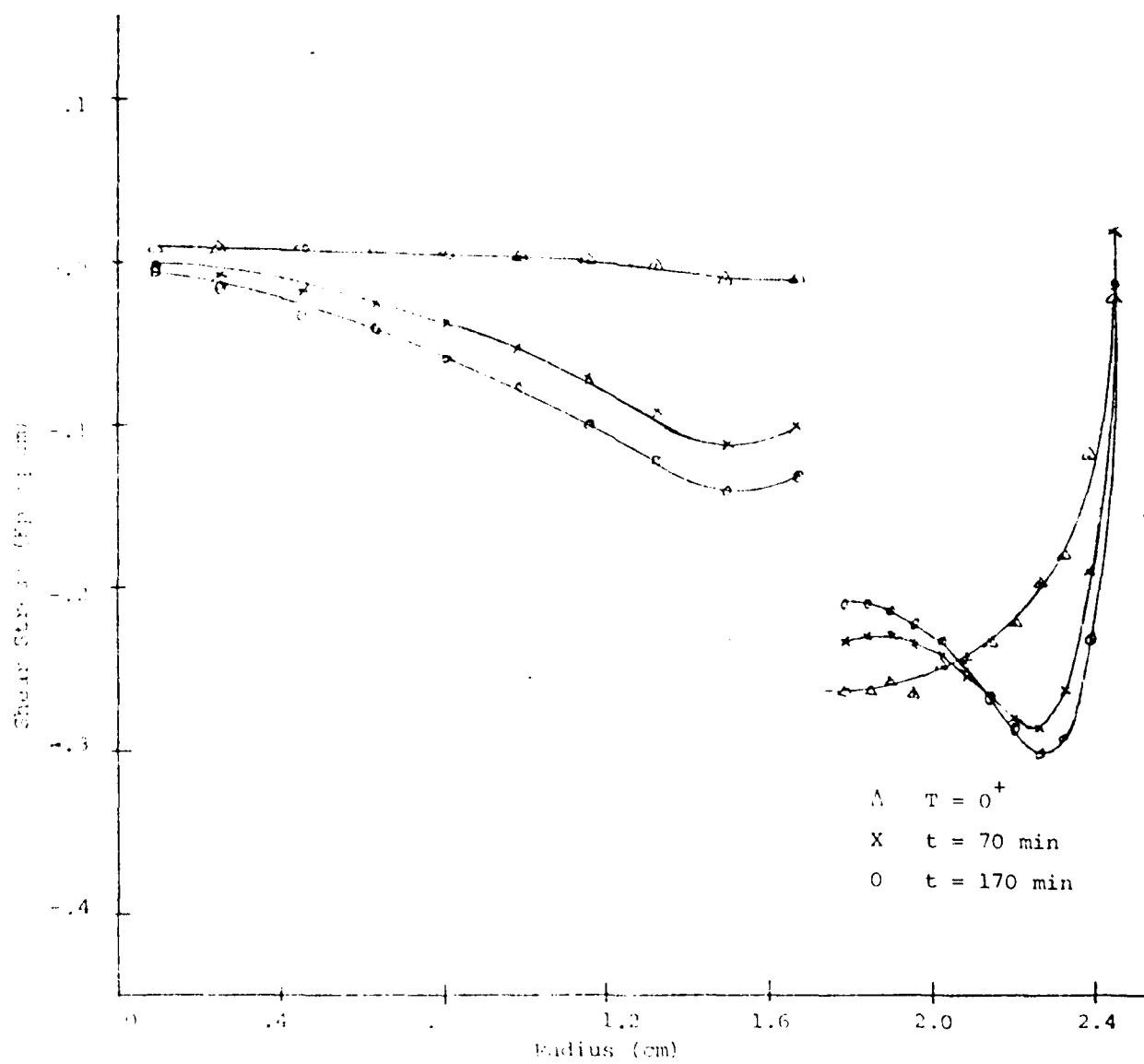
Fig 4.6-E.   Hoop Stress, Disc.
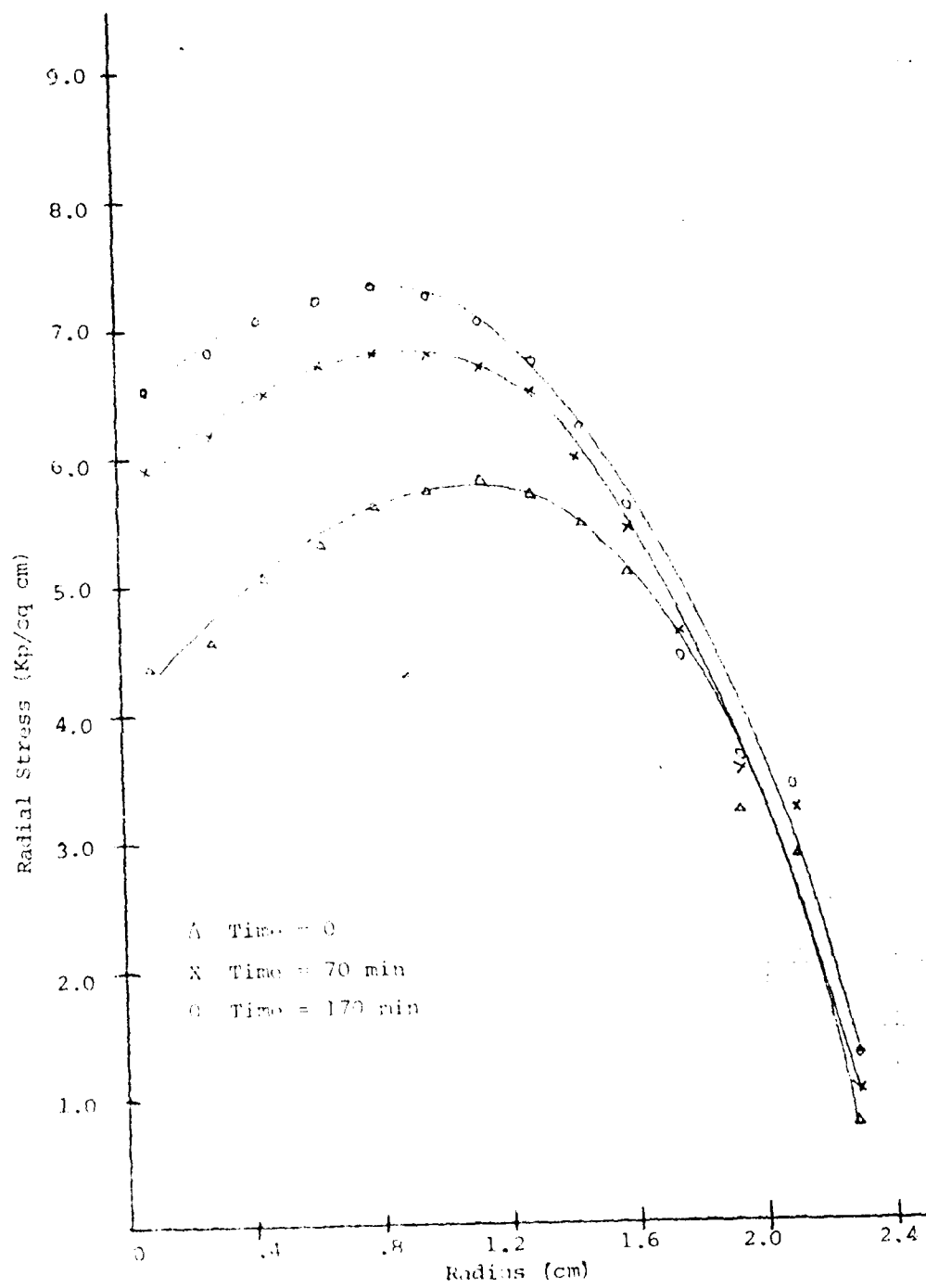
Fig 4.6-F.   Shear Stress, Disc.
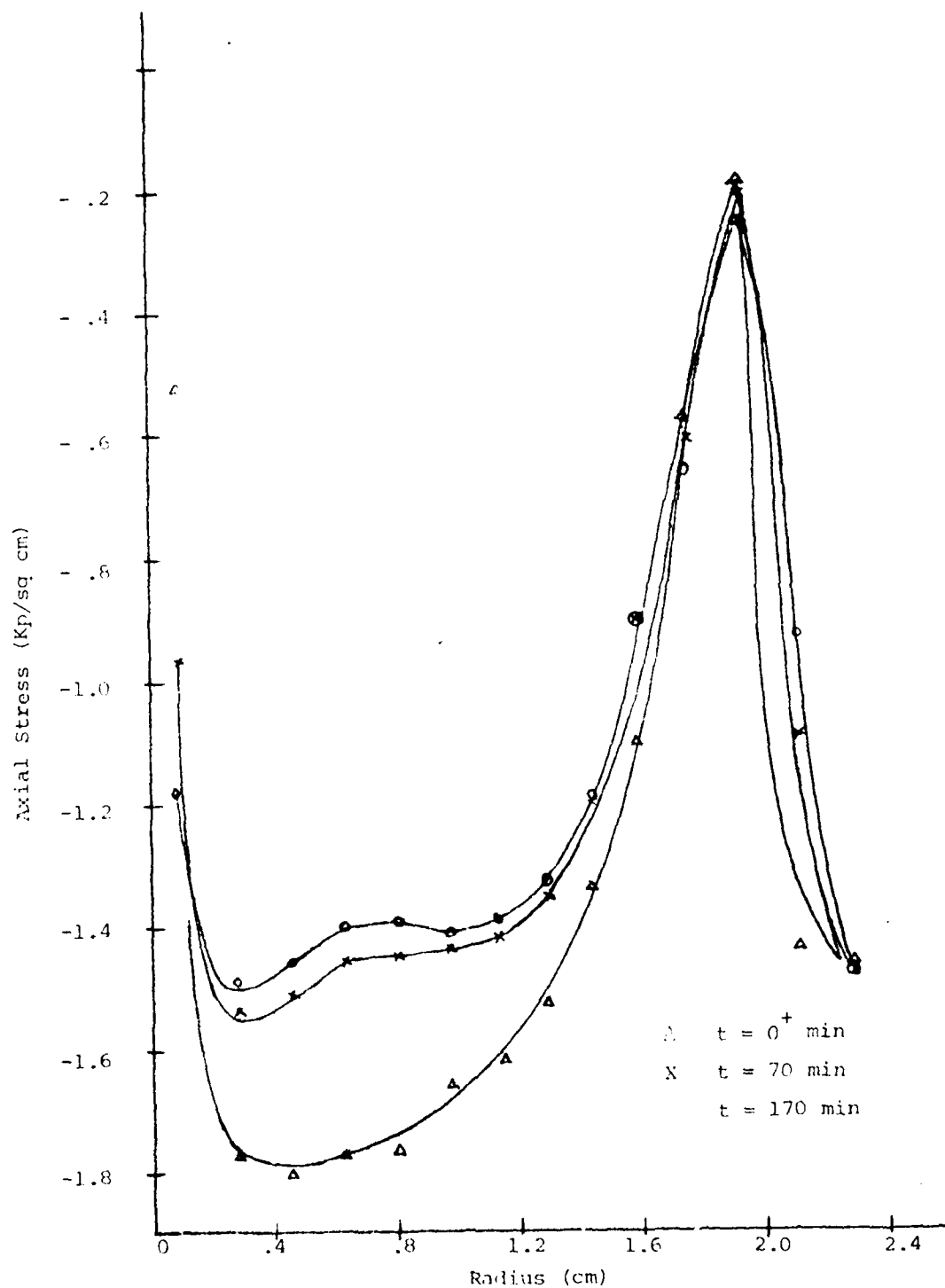
Fig 4.6-G.   Radial Stress, End Plate.

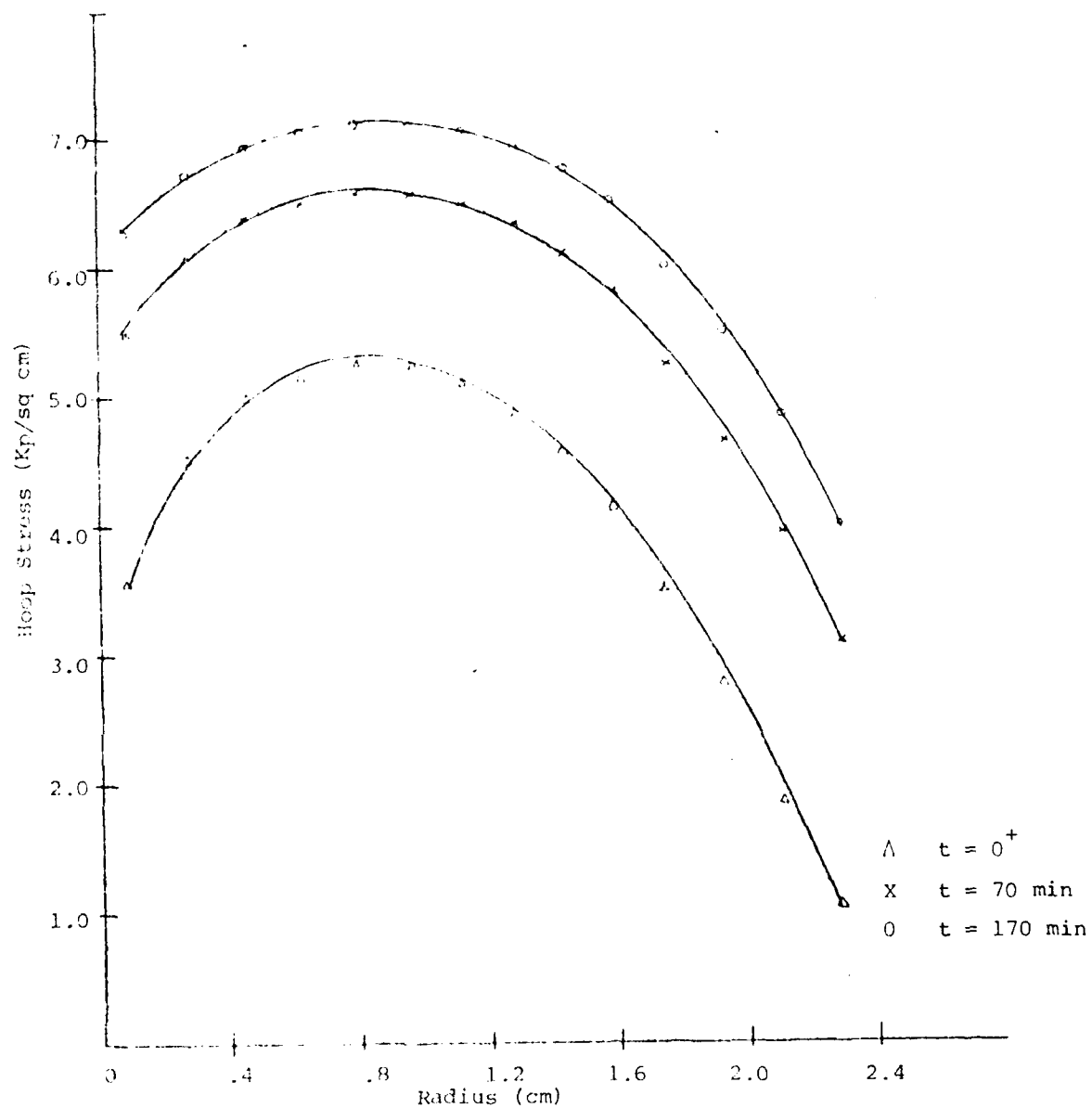Fig 4.6-H. Axial Stress, End Plate.
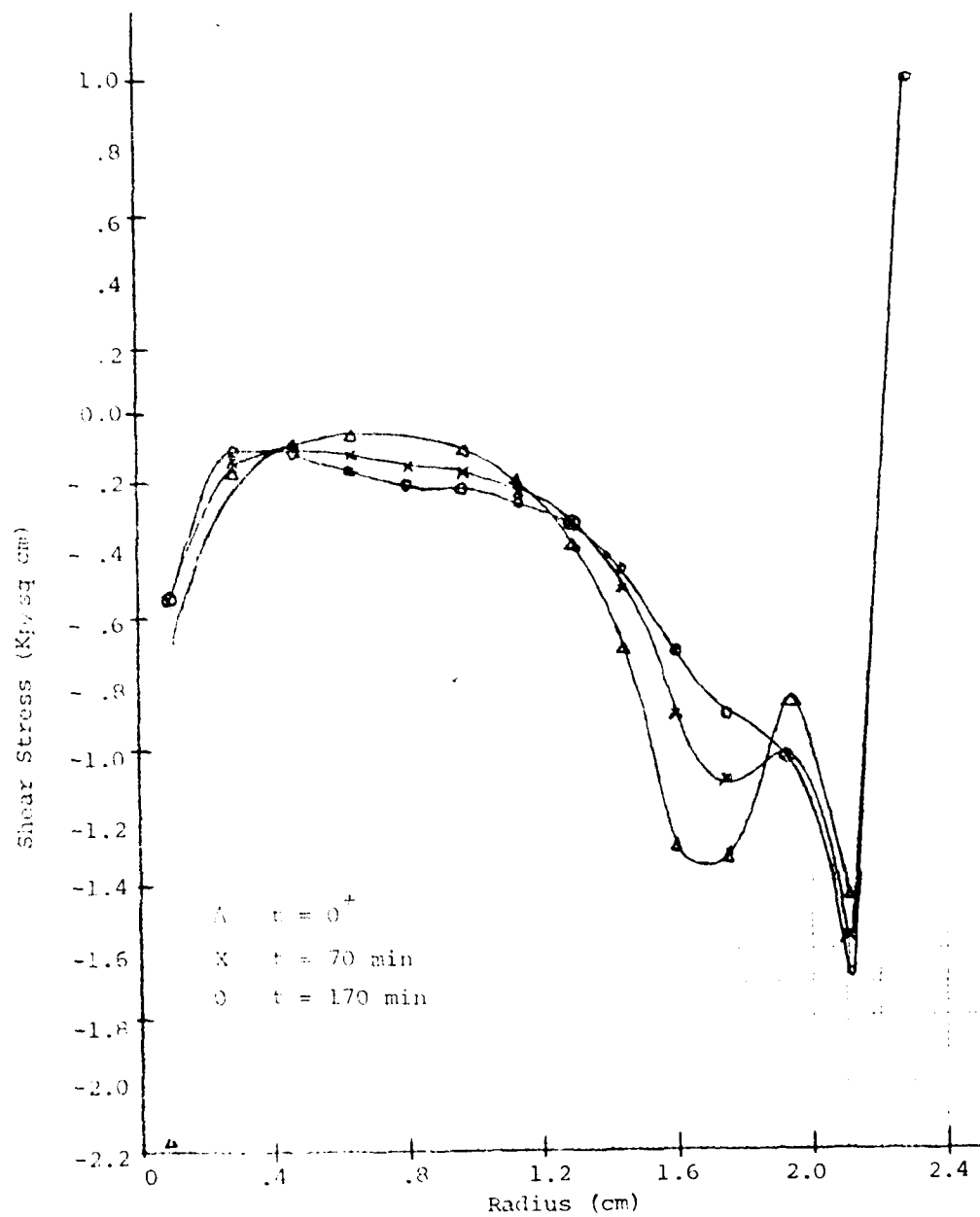
Fig 4.6-I. Hoop Stress, Endplate.

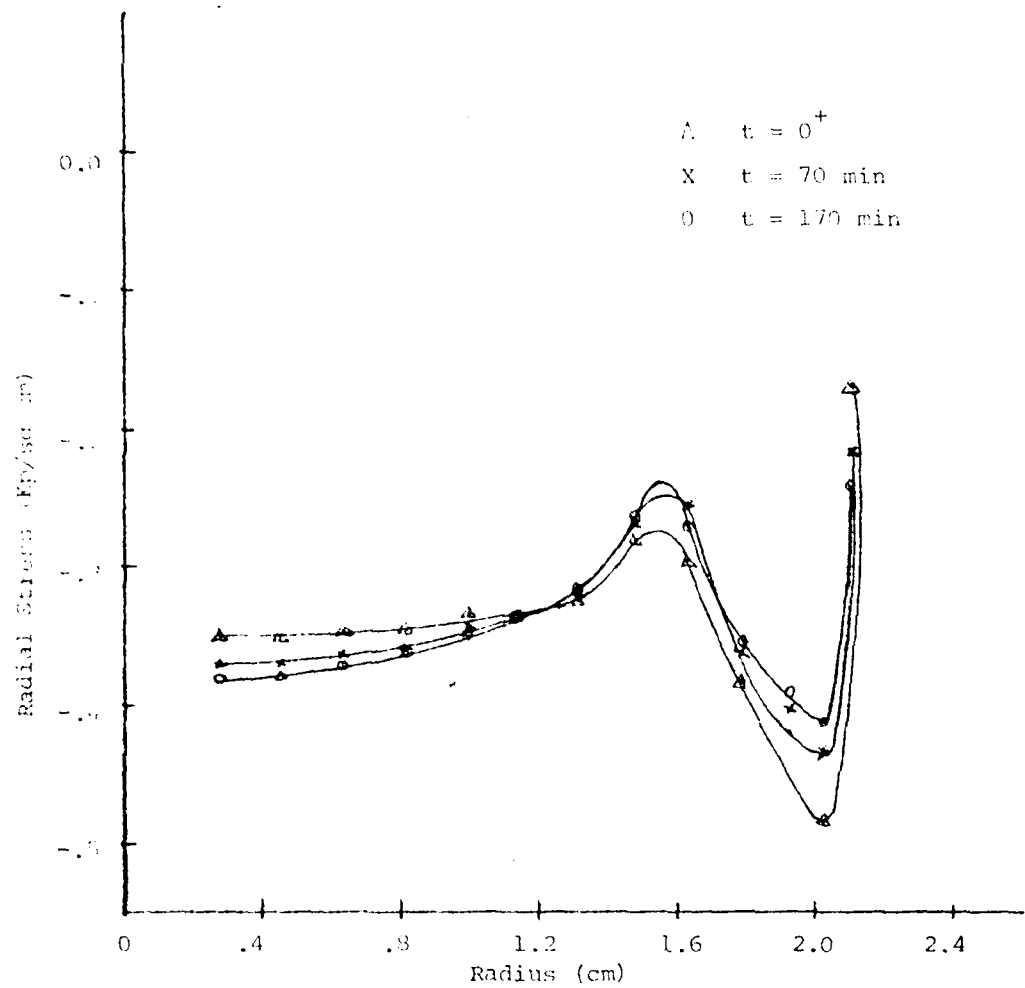Fig 4.6-J.   Shear Stress, End Plate.
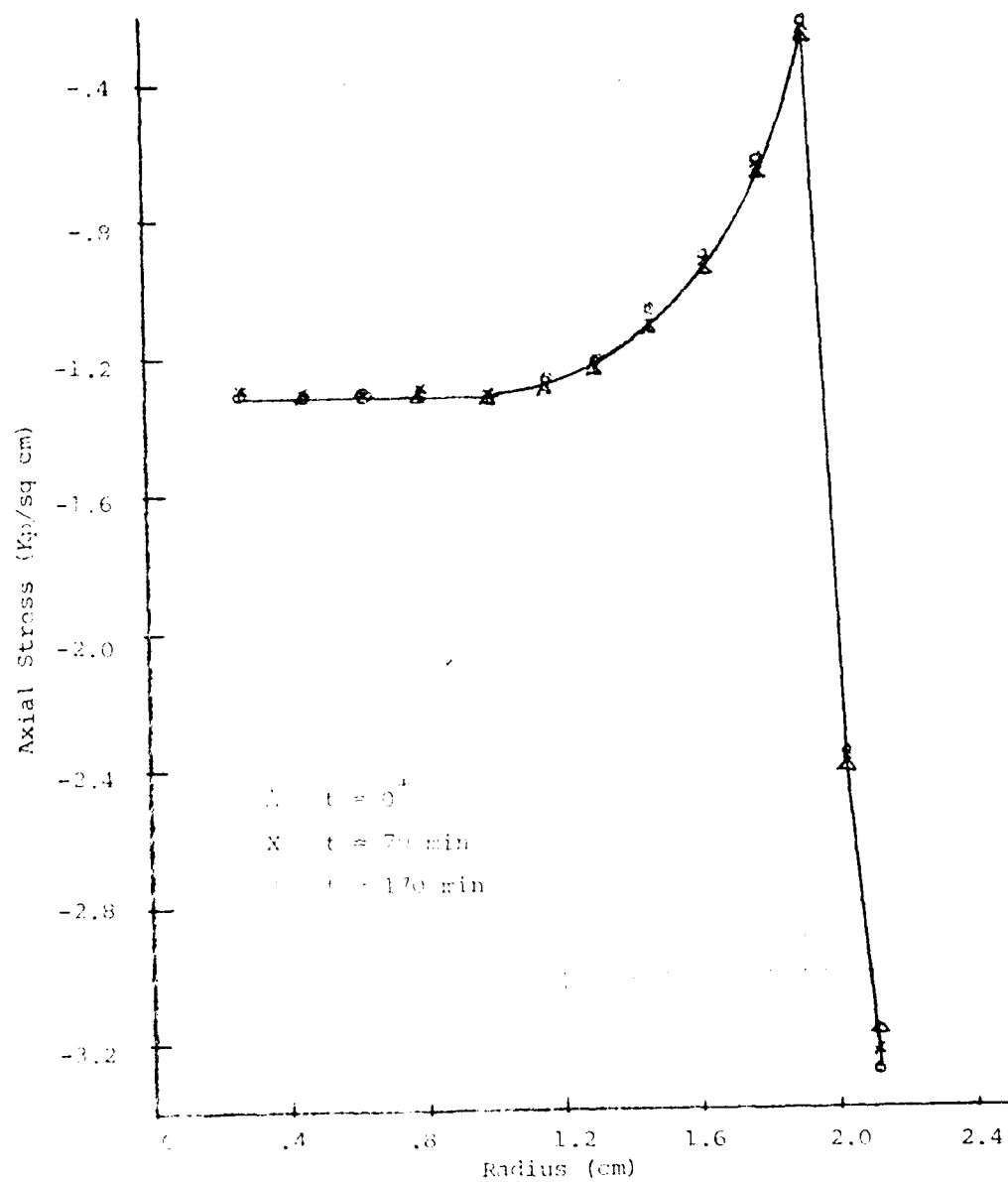
Fig 4.6-K. Radial Stress - Vertebral Body.

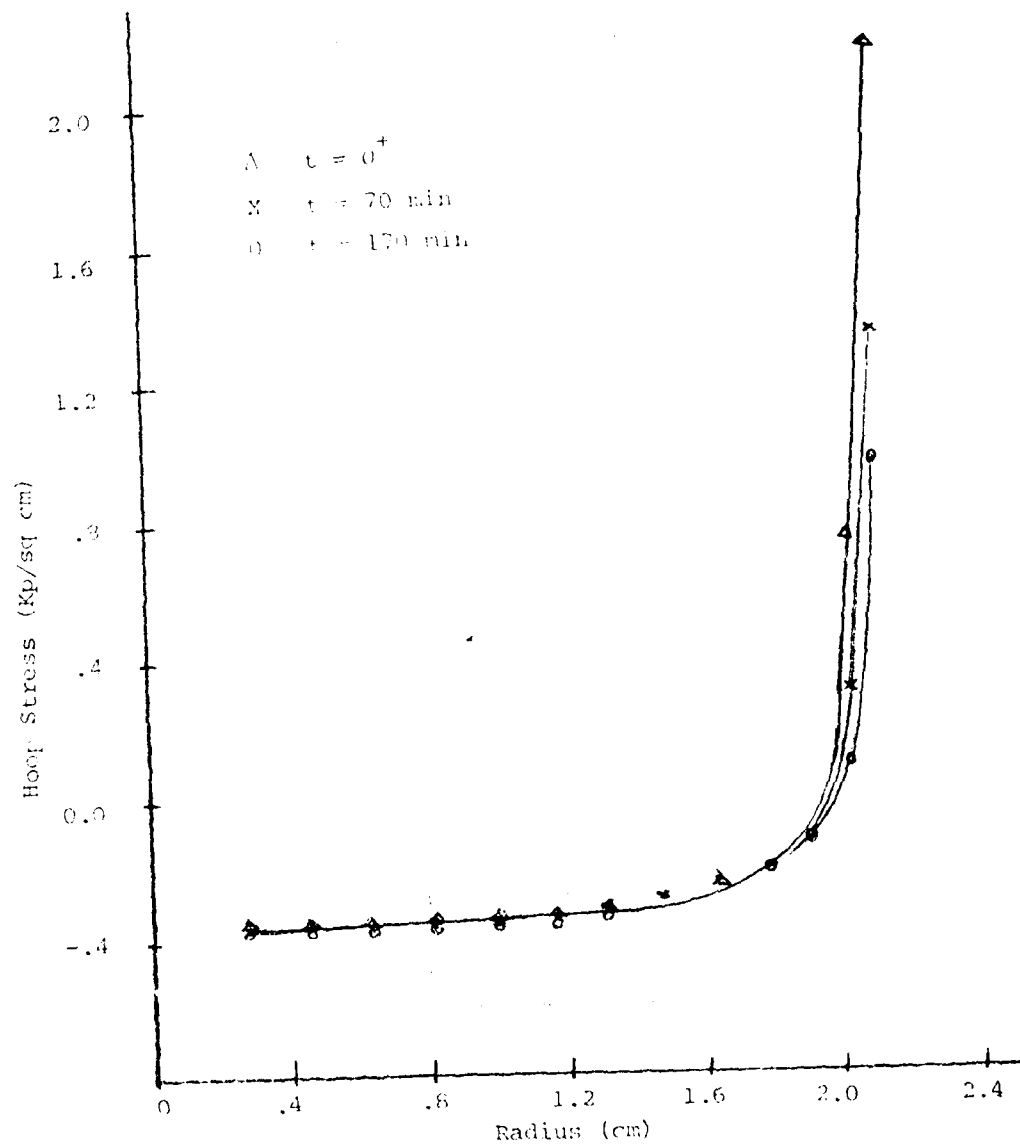Fig 4.6-L.   Axial Stress, Vertebral Body.
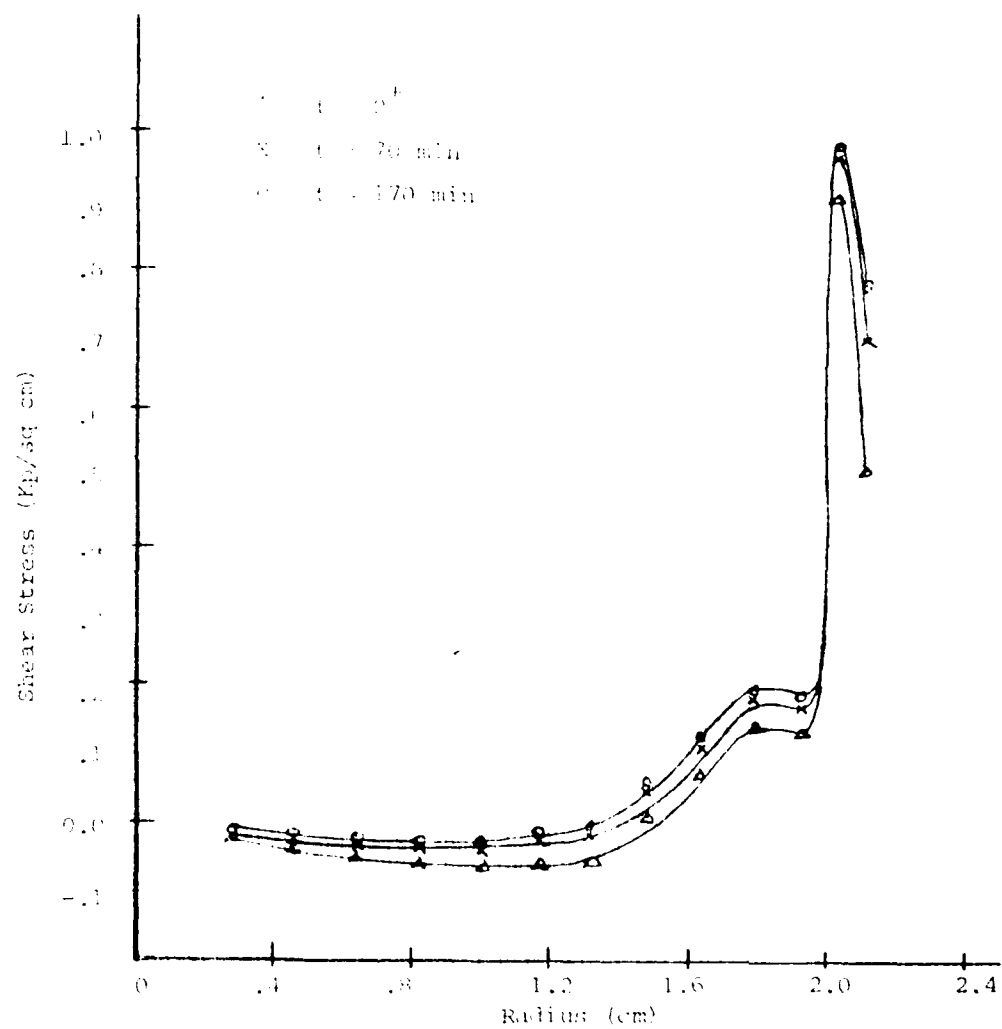
Fig 4.6-M. Hoop Stress, Vertebral Body.

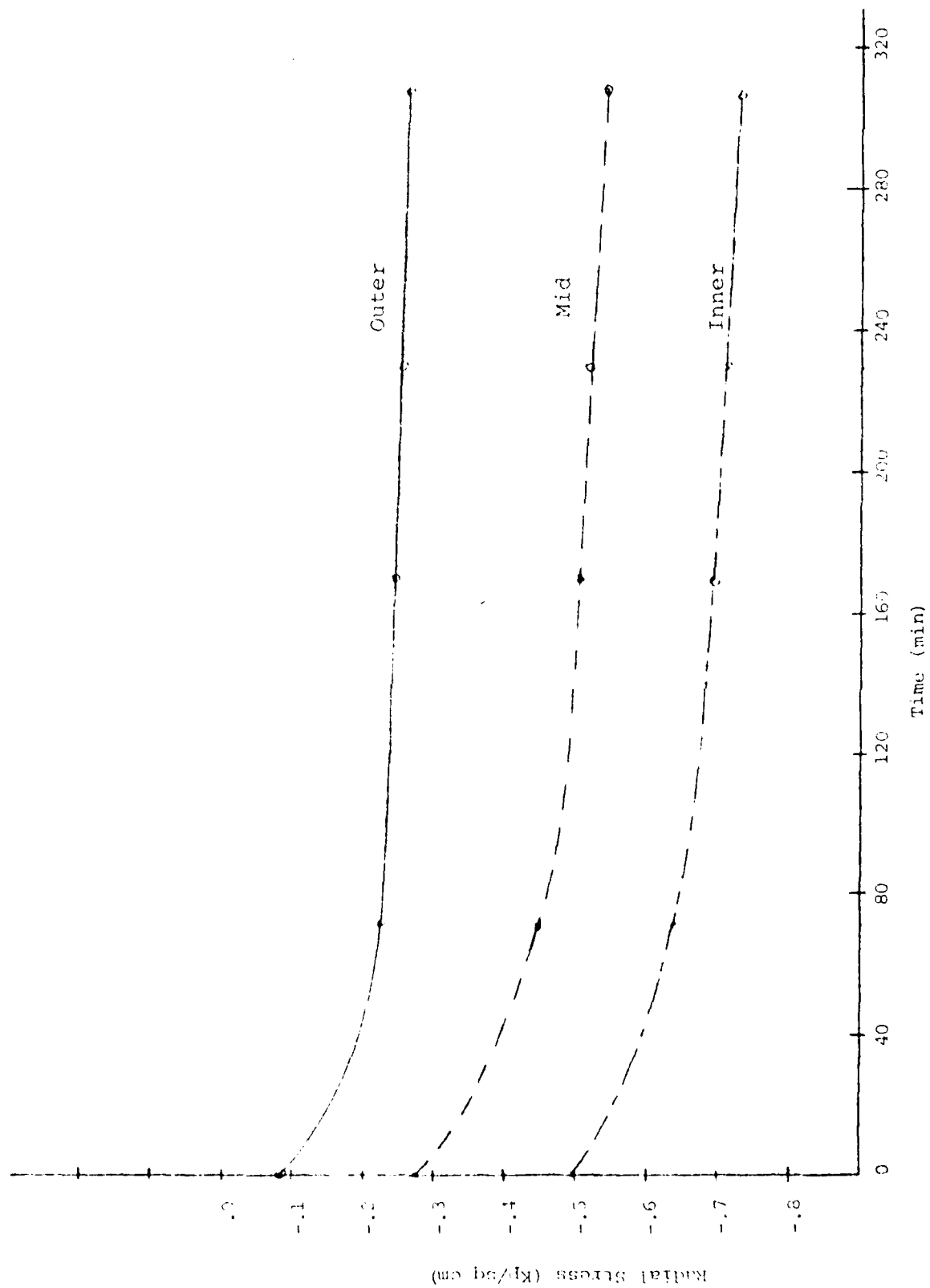Fig 4.6-N. Shear Stress, Vertebral Body.

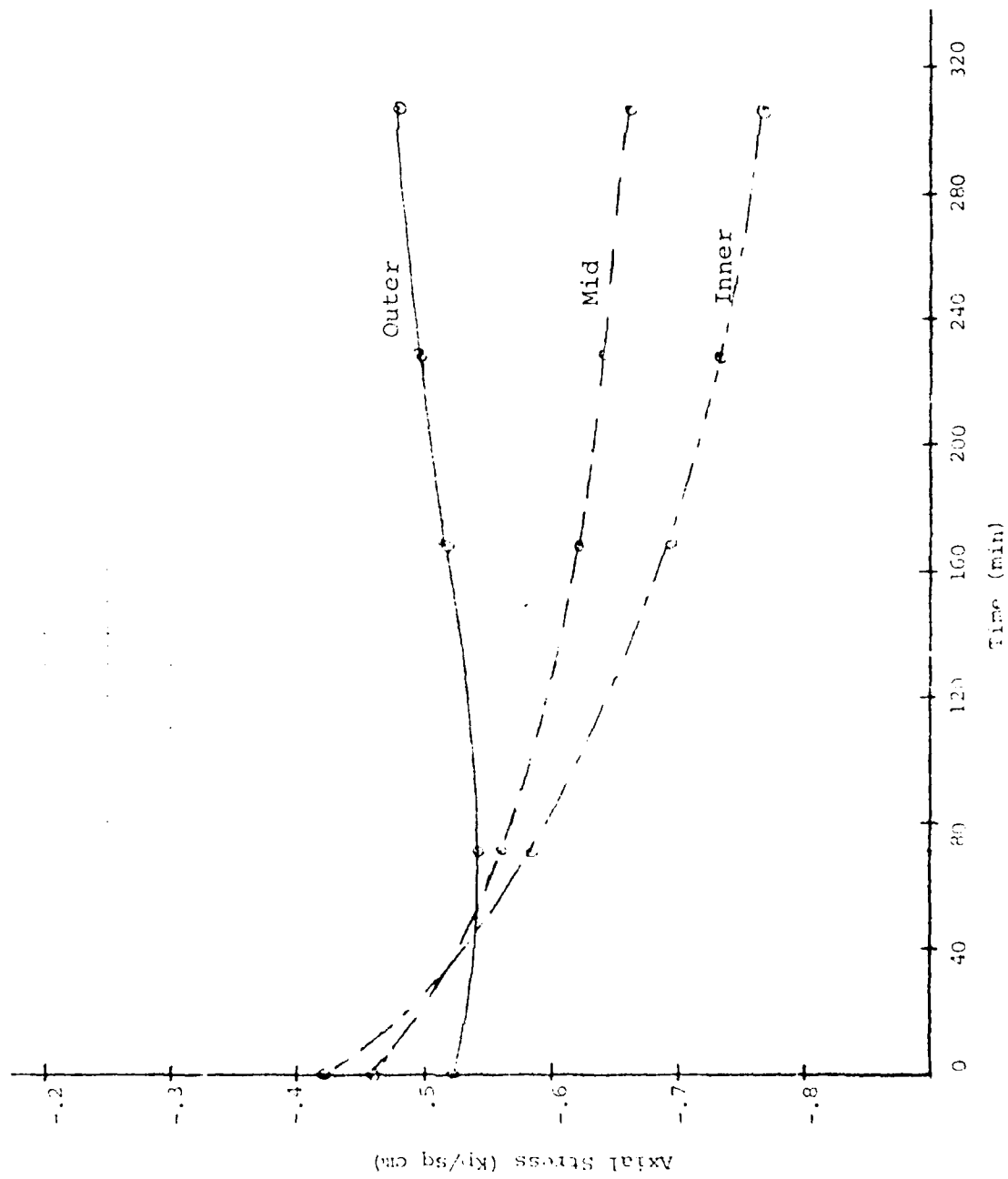Fig 4.6-O. Radial Ply Stress.

73
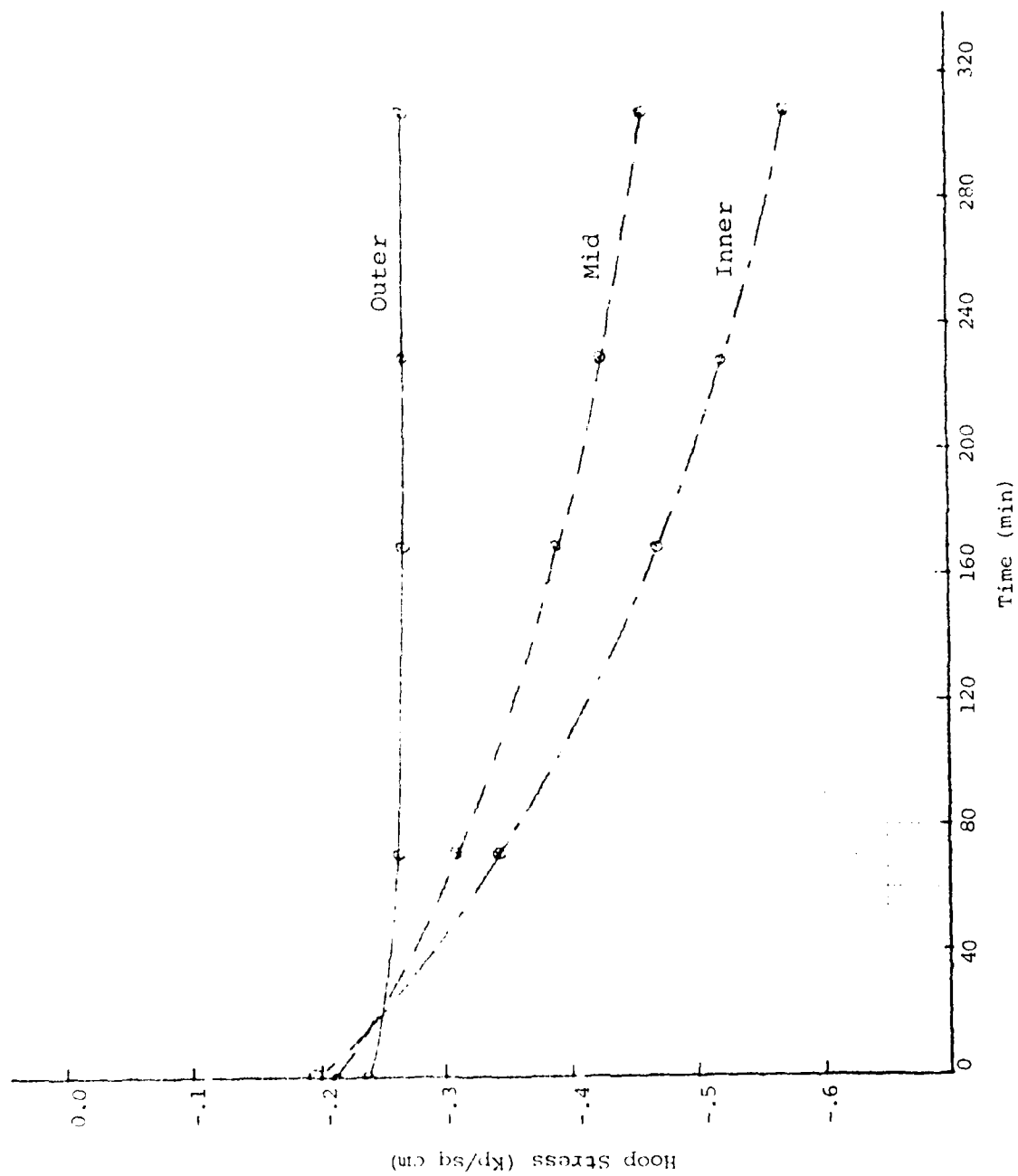
Fig 4.6-P. Axial Ply Stress.
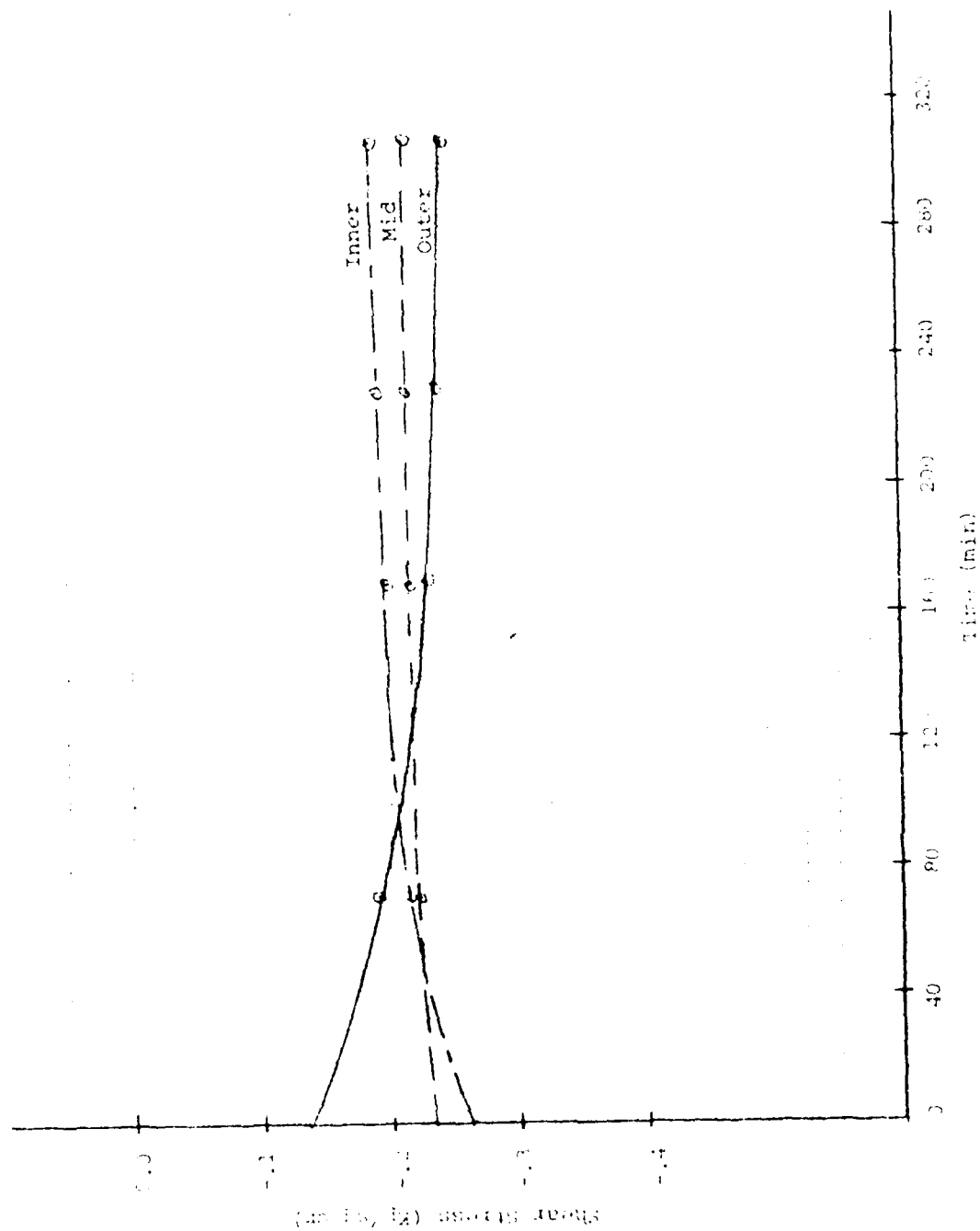
74

Fig 4.6-Q. Hoop Ply Stress.

75

Fig 4.6-R. Shear Ply Stress.

V. CONCLUSION

The mechanical behavior of the intervertebral joint can be realistically modelled through the use of the finite element method. By matching one-dimensional experimental displacement data material parameters are determined which provide a good overall description of the time dependent behavior of the joint.

The inclusion of the orthotropic material properties of the annulus in the model caused significant stress redistributions throughout the disc. These redistributions indicate the importance of the annulus as a restraining mechanism on the outward flow of the nucleus under axial loading. It is concluded that the orthotropic nature of the annulus is a factor which should be included when modelling the intervertebral joint.

The results of this study indicate that both the nucleus pulposis and the annulus fibrosis are visco-elastic materials. The initial assumption that the experimentally observed creep response of the joint was due to the nucleus alone proved unworkable. It was found that the creep behavior of the joint could be simulated only if both the nucleus and the annulus were modelled visco-elastically. Due to the limitations of the curve matching technique, unique values for the visco-elastic parameters in these regions cannot be determined. Determination of unique

parameters would require at least two-dimensional displacement data, which at present is unavailable.

Examination of the displacement profiles and stress redistributions within the model provides insight into the internal behavior of the joint under axial loading. It was found that the cortical bone which encases the vertebral body behaves essentially like a shell subjected to internal pressure. On the other hand, the geometry of the thoracic disc is such that the annulus behaves like an axially loaded ring. Under small loads, the inner lamellae of the annulus do most of the work in restraining the outward flow of the nucleus. It appears that when the joint is subjected to axial compression, the load is transmitted mainly through the cortical shell and end plates to the nucleus, which then acts as the primary load carrying structure of the joint.

BIBLIOGRAPHY

1. Belytschko, T., Kulak, R. F., Schultz, A. B., and Galante, J. O., "Finite Element Stress Analysis of an Intervertebral Disc," _Journal of Biomechanics_, Vol. 7, pp. 277-285, 1974.

2. Broberg, K. B. and Von Essen, H. O., "Modeling of Intervertebral Discs," _Spine_, Vol. 5, No. 2, 1980.

3. Brown, T., Hanson, R. J., and Yorra, A. J., "Some Mechanical Tests on the Lumbosacral Spine With Particular Reference to the Intervertebral Disc," _Journal of Bone and Joint Surgery_, Vol. 39A, pp. 1135-1164, 1957.

4. Burns, M. L., "Analytical Modelling of Load Deflection Behavior of Intervertebral Discs Subjected to Axial Compression," AFOSR-TR-79-0795, July 1979.

5. Burns, M. S. and Kaleps, I., "Analysis of Load-Deflection Behavior of Intervertebral Discs Under Axial Compression Using Exact Parametric Solutions of Kelvin-Solid Models," _Journal of Biomechanics_, Vol. 13, pp. 959-964, 1980.

6. Flugge, W., _Viscoelasticity_, Waltham, Mass., Blaisdell Publishing Company, 1967.

7. Galante, J. O., "Tensile Properties of the Human Lumbar Annulus Fibrosis," _Acta Orthop. Scand._, Supplement 100, 1967.

8. Hickey, D. S. and Hukins, D. W. L., "Relation Between the Structure of the Annulus Fibrosis and the Function and Failure of the Intervertebral Disc," _Spine_, Vol. 5, No. 2, 1980.

9. Hinnerichs, T., _Viscoplastic and Creep Crack Growth Analysis by the Finite Element Method_, Ph.D. Dissertation, presented to the Aeronautics and Astronautics Department: Air Force Institute of Technology, June 1980.

10. Hinrichsen, R. L., _A Viscoelastic Finite Element Model of the Human Intervertebral Joint_, Thesis, Wright-Patterson Air Force Base, Air Force Institute of Technology, 1980.

11. Horton, W. G., "Further Observations on the Elastic Mechanism of the Intervertebral Disc," Journal of Bone and Joint Surgery, Vol. 40B, No. 3, 1958.

12. Jones, R. M., Mechanics of Composite Materials, Scripta Book Company, Washington, D.C., 1975.

13. Kazarian, L. E., "Creep Characteristic of the Human Spinal Column," Orthop. Clinics of North America, Vol. 6:1, January 1976.

14. Kazarian, L. E. and Kaleps, I., "Mechanical and Physical Properties of the Human Intervertebral Joint," AMRL-TR-79-3, June 1979.

15. Kulak, R. F., Belytschko, T. B., and Schultz, A. B., "Nonlinear Behavior of the Human Intervertebral Disc Under Axial Load," Journal of Biomechanics, Vol. 9, pp. 377-386, 1976.

16. Lin, H. S., Liu, Y. K., and Adams, K. H., "Mechanical Response of the Lumbar Intervertebral Joint Under Physiological (Complex) Loading," Journal of Bone and Joint Surgery, Vol. 60A, pp. 41-54, 1978.

17. Markolf, K. L., "Deformation of the Thoracolumbar Intervertebral Joints in Response to External Loads," Journal of Bone and Joint Surgery, Vol. 54-A, No. 3, 1972.

18. Nachemson, A., "Lumbar Intradiscal Pressure," Acta Orthop. Scand., Supplement 43, 1960.

19. Nachemson, A. L., Schultz, A. B., and Berkson, M. H., "Mechanical Properties of Human Lumbar Spine Motion Segments, Influences of Age, Sex, Disc Level, and Degeneration," Spine, Vol. 4, No. 1, 1979.

20. Rolander, S. D., "Motion of the Lumbar Spine With Special Reference to the Stabilizing Effect of Posterior Fusion," Thesis, Acta Orthop. Scand., Supplement 90, 1966.

21. Spilker, R. L., "A Simplified Finite Element Model of the Intervertebral Discs," Spine, Vol. 5, No. 2, 1980.

22. Swanson, S. A. V., "Biomechanical Characteristics of Bone," Advances in Biomedical Engineering, Vol. I, Academic Press, Inc., New York, NY, 1971.

23.   Zienkiewicz, O. C., Watson, M., and King, I. P., "A Numerical Method of Visco-Elastic Stress Analysis," Int. J. Mech. Sci., Vol. 10, pp. 807-827, 1968.

24.   Zienkiewicz, O. C., The Finite Element Method, 3rd Edition, Maidenhead, Berkshire, England, McGraw-Hill Book Co., Ltd., 1977.

VITA

Leslie Jean Allen was born on 15 November 1952 in Pontiac, Michigan. She graduated from high school in Bloomfield Hills, Michigan in 1970 and attended the University of Michigan from which she received the degree of Bachelor of Aerospace Engineering in May 1974. Upon graduation, she received a commission in the United States Air Force through the ROTC Program. She attended the Aircraft Maintenance Office. Course at Chanute Air Force Base, Illinois, graduating in December 1974. She served one year as an aircraft maintenance officer in the 4950th Field Maintenance Squadron at Kirtland Air Force Base, New Mexico. This was followed by two consecutive overseas tours. She was assigned to the 610th Military Airlift Support Squadron at Yokota Air Force Base, Japan as a maintenance officer on C-130, C-141, and C-5 aircraft from June 1976 to March 1978. She attended Squadron Officer School in residence during the Spring of 1978. From June 1978 to May 1980, she served as a maintenance officer on F-111 aircraft at RAF Lakenheath, England. In May 1980 she entered the Air Force Institute of Technology at Wright-Patterson Air Force Base, Ohio to pursue a M.S. degree in Aeronautical Engineering.

REPORT DOCUMENTATION PAGE		READ INSTRUCTIONS BEFORE COMPLETING FORM
1. REPORT NUMBER AFIT/GAE/AA/81D-1	2. GOVT ACCESSION NO. AD-A111 161	3. RECIPIENT'S CATALOG NUMBER
4. TITLE (and Subtitle) Finite Element Analysis of the Visco-Elastic Interaction of the Annulus Fibrosis and Nucleus Pulposis Within the Human Intervertebral Joint		5. TYPE OF REPORT & PERIOD COVERED M.S. Thesis
		6. PERFORMING ORG. REPORT NUMBER
7. AUTHOR(s) Leslie J. Allen Captain		8. CONTRACT OR GRANT NUMBER(s)
9. PERFORMING ORGANIZATION NAME AND ADDRESS Air Force Institute of Technology (AFIT-EN) Wright-Patterson Air Force Base, Ohio 45433		10. PROGRAM ELEMENT, PROJECT, TASK AREA & WORK UNIT NUMBERS
11. CONTROLLING OFFICE NAME AND ADDRESS Air Force Aerospace Medical Research Laboratory Wright Patterson Air Force Base, Ohio 45433		12. REPORT DATE December 1981
		13. NUMBER OF PAGES 82
14. MONITORING AGENCY NAME & ADDRESS(If different from Controlling Office)		15. SECURITY CLASS. (of this report) Unclassified
		15a. DECLASSIFICATION DOWNGRADING SCHEDULE

16. DISTRIBUTION STATEMENT (of this Report)

Approved for Public Release; Distribution Unlimited

17. DISTRIBUTION STATEMENT (of the abstract entered in Block 20, if different from Report)

20 JAN 1982

18. SUPPLEMENTARY NOTES

Approved for public release; IAW AFR 190-17

Frederic Lynch, Major, USAF   Air Force Institute of Technology (ATC)
Director of Public Affairs   Wright-Patterson AFB, OH 45433

19. KEY WORDS (Continue on reverse side if necessary and identify by block number)

Finite Element
Visco-Elastic
Intervertebral Joint
Annulus Fibrosis

20. ABSTRACT (Continue on reverse side if necessary and identify by block number)

An understanding of the mechanical properties and behavior of the intervertebral disc is critical to several current areas of research. Among these are the study of the effects of extreme gravitational forces on the air crews of high performance aircraft and the related problem of spinal injuries due to aircraft ejection. This study was undertaken in order to construct a realistic analytical model of the intervertebral joint using the finite element approach.

DD FORM 1473 EDITION OF 1 NOV 65 IS OBSOLETE
1 JAN 73

Experiments have shown that healthy intervertebral joints exhibit creep when subjected to axial load. The focus of this investigation is the behavior and interaction of the nucleus and annulus under loading. An axisymmetric finite element model is employed which incorporates a linear visco-elastic constitutive relation for the annulus and nucleus, based upon a three-parameter Kelvin solid. The visco-elastic constants are found by matching one-dimensional axial experimental data with this two dimensional model. The nucleus, which is composed of a series of concentric lamellae of collagen fibers, has been modelled as a 12 ply structure of orthotropic material.

Results are presented which depict the displacement profiles and stress redistributions occurring as a consequence of the interaction of the annulus, nucleus, and bony end plate under axial compressive loading. These profiles clearly show the importance of the nucleus as a load carrying structure and the action of the annulus in restraining the outward flow of the nucleus. Also presented are the variations in stress with time in three of the lamina of the annulus. Results indicate that the orthotropic material properties of the annulus have a significant impact upon its time dependent behavior and should be included when modelling the joint.